OLD DOMINION UNIVERSITY RESEARCH FOUNDATION

DEPARTMENT OF MECHANICAL ENGINEERING AND MECHANICS
SCHOOL OF ENGINEERING
OLD DOMINION UNIVERSITY
NORFOLK, VIRGINIA

COMPARATIVE STUDY OF FLARE CONTROL LAWS

By

A. A. Nadkarni

Principal Investigator: W. J. Breedlove, Jr.

Progress Report
For the period December 15, 1977 - December 14, 1978

Prepared for the
National Aeronautics and Space Administration
Langley Research Center
Hampton, Virginia

Under
Research Grant NSG 1480
J. F. Creedon, Technical Monitor
Flight Electronics Division

February 1979

DEPARTMENT OF MECHANICAL ENGINEERING AND MECHANICS
SCHOOL OF ENGINEERING
OLD DOMINION UNIVERSITY
NORFOLK, VIRGINIA

COMPARATIVE STUDY OF FLARE CONTROL LAWS

By

A. A. Nadkarni

Principal Investigator: W. J. Breedlove, Jr.

Progress Report
For the period December 15, 1977 - December 14, 1978

Prepared for the
National Aeronautics and Space Administration
Langley Research Center
Hampton, Virginia 23665

Under
Research Grant NSG 1480
J. F. Creedon, Technical Monitor
Flight Electronics Division

Submitted by the
Old Dominion University Research Foundation
P. O. Box 6369
Norfolk, Virginia 23508

February 1979

TABLE OF CONTENTS

LIST OF TABLES

LIST OF FIGURES

(cont'd)

LIST OF FIGURES (CONT'D)

(cont'd)

LIST OF FIGURES (CONCL'D)

COMPARATIVE STUDY OF FLARE CONTROL LAWS

By

A. A. Nadkarni[1]

1. INTRODUCTION

The purpose of this report is to present the development of a digital 3-D automatic control law designed to achieve an optimal transition of a B-737 aircraft between various initial glide slope conditions and the desired final touchdown condition. The digital control law developed here is essentially a time-invariant state-estimate feedback law, and the design procedure is capable of using the Microwave Landing System (MLS) under development by the Federal Aviation Agency (FAA). The study of a curved flight path leading to a steep final approach and touchdown under low visibility conditions is part of the Terminally Configured Vehicle (TVC) program, sponsored by NASA/Langley Research Center. The goals of this program include the reduction of aircraft noise in communities surrounding airports, the reduction of fuel consumption, the reduction of the effects of adverse weather conditions on aircraft operations, and the efficient use of airspace in congested terminal areas through the use of the Microwave Landing System. Another goal is to increase the overall efficiency of the operation in the final phase of the flight (approach and landing) by reducing the heavy workload on the pilot by automating as many routine operations as possible.

The major reason for the use of steep glide slopes is the resultant noise reduction in comparison with the currently used 2.5° to 3° glide slopes with the Instrument Landing System (ILS). The steeper glide slope reduces the noise levels perceived on an identical segment of the ground for two reasons. First, at equal distances from the touchdown point, the aircraft flying a steeper, say a 6° glide slope, is at about twice the altitude compared to that flying a 3° glide slope. This difference in altitude causes a considerable reduction in the noise level perceived on

---

[1] Research Assistant Professor, Old Dominion University Research Foundation, P. O. Box 6369, Norfolk, Virginia 23508.

the ground even if the two sources generate identical noise levels. Second, an aircraft flying a steeper glide slope requires a lower thrust setting, and this causes further reduction in the noise level perceived on the ground. The reduction in thrust setting has the added advantage of reducing the fuel consumption during the final phase of the flight path. The ability to fly varying glide slopes may also provide an effective method to avoid encountering vortices generated by larger aircraft. This versatility may result in a more efficient use of the airspace.

The use of steeper glidepaths in the final phase is not without its attendent disadvantages. The lower thrust setting and the higher sink rates allow considerably less reaction time for the pilots to take any corrective actions in the event of atmospheric disturbances, mechanical failures of the system, etc. In these circumstances, the role of an automatic control law to relieve the pilot of the routine workload can be appreciated to its greatest extent.

The need for reducing touchdown dispersion in the presence of varying flight conditions encountered also emphasizes the desirability of an automatic control law during the flare portion of the landing. The reduction in the touchdown dispersions greatly facilitates high-speed rollout, which significantly increases the traffic handling capacity of the terminal.

In the earlier work (ref. 1), a discrete, optimal control law to achieve an optimal transition (from the initial glide slope to the required touchdown conditions) was designed with time-varying gains. As the time-varying control law is difficult to implement in practice onboard the aircraft, development of a constant-gain control law was undertaken (ref. 2) and is implemented with a slight modification in the present study. The modification consists in defining the elevator position (δe) as one of the states rather than one of the control variables as was done in previous studies (refs. 1 to 4). The elevator rate ($\dot{\delta e}$) is now defined as a control variable. This change was done mainly because of the need to study the open-loop responses with an elevator linearly varying with time (a ramp) forced on the system.

In section 3, the mathematical model used for describing the deviations of the aircraft's longitudinal variables from their steady-state values is

briefly described. The effect of lags in the thrust buildup are included in the model by assuming a linear dynamical model for the thrusters (engines). A new method of including the effects of steady winds, wind shears and gusts is also indicated. The model is expressed in state variable form, which is suitable for application of modern control theory techniques. The development of the model follows closely the development of the model outlined in references 1 to 6. However, the new wind model is shown to be a more realistic one in that it can model the shear profiles that are normally given in practice as spatial profiles rather than temporal profiles. In addition, it is also shown that the new model overcomes the uncontrollability problem posed by the previous model.

In section 4, the design procedure to compute a digital, time-invariant, optimal control law for a discrete regulator problem is presented. The method is extended to compute two forms of control laws to evaluate the discrete regulator acted upon by constant disturbance.

In section 5, the performance curves are presented using the above control laws for the following cases:

(1) optimal flare in absence of winds,
(2) glide slope tracking in presence of specified wind profiles,
(3) optimal flare in presence of wind profiles, and
(4) flare to achieve transition from initial glideslope to touchdown conditions with open-loop control law forced on the system.

Finally, in section 6, the conclusions derived from the present study, the relative merits of various control schemes, and suggestions for overcoming certain difficulties encountered are listed.

2. NOMENCLATURE

A	system matrix, continuous time case
B	control effort matrix, continuous time case
C_{wg}	transformation matrix, body to stability frame
C_{ws}	transformation matrix, inertial to stability frame
F	state transition matrix, discrete time case

G	control effort matrix, discrete time case
H	constant gain matrix, discrete time case
J	quadratic performance index
P	Riccati matrix
Q	state weighting matrix
q	integral states
R	control weighting matrix
S	control-rate weighting matrix
U_i	horizontal component of inertical velocity V_i
u	control vector, perturbation in horizontal velocity
W	eigen vector matrix
W_i	vertical component of inertial velocity V_i
W_d	constant disturbance vector
W_g	wind gust vector, body frame
W_s	steady wind vector, inertial frame
w	wind vector in stability frame, perturbation in vertical velocity
$ox_e y_e z_e$	frame parallel to earth-fixed (vertical) frame
$ox_b y_b z_b$	body-fixed frame
$ox_s y_s z_s$	stability frame
X	shear rate in horizontal wind velocity, kn/100 ft (1 kn = 0.514 m/sec; 100 ft = 30.48 m)
x	state variable vector
Z	shear rate in vertical wind velocity, kn/100 ft (1 kn = 0.514 m/sec; 100 ft = 30.48 m)
	controlled variable vector
ξ	white noise process

Subscripts

b	body-fixed frame
f	final, terminal
g	gust components
i	inertial vector
o	initial, nominal
s	stability frame
w	wind components, constant disturbance
∞	steady-state value

Superscripts

I	components in inertial frame
s	components in stability frame
( )'	normalized
$\overline{(\ )}$	augmented

3. DESCRIPTION OF THE SYSTEM MODEL

The development of the mathematical model in this study follows closely the development of a similar model described in detail in references 1 to 6. The complete derivation of the system equations is described in these references; however, a brief outline of the derivation is given below for the sake of completeness.

3.1. Aircraft Dynamics with Wind Disturbances

This study is concerned only with the final phase of flight, viz the flare. Thus, the aircraft is approaching the runway on a certain initial glidepath. The aircraft is aligned with the runway, has a zero or at most a very small yaw angle with respect to the runway, as well as a zero bank (or roll) angle, except in the case of a significant crosswind. Therefore,

all the lateral dynamics are neglected during the analysis and only longitudinal dynamics are considered.

With the assumptions stated above and assuming small perturbations about the nominal path, the nonlinear equations of motion of the aircraft can be linearized using well-known methods. The complete equations of motion and the linearization procedure are outlined in references 5 to 7. These nonlinear equations are derived assuming (1) a flat earth, (2) an earth-fixed frame of reference, (3) a rigid aircraft, and (4) second-order terms are neglected. These equations of motion are coupled. However, for a steady-state flight condition, the equations can be decoupled into two groups, the longitudinal equations and the lateral equations of motion. As indicated above, we deal with only longitudinal equations of motion in this study.

The decoupled, nonlinear longitudinal equations of motion are then linearized about the nominal trajectory (i.e. the steady-state flight of -3°, -6° glide slope, etc.) to obtain the linear perturbative equations in the state variable form. The equations are expressed in a stability axes coordinate frame attached to the aircraft at the center of mass.

The final linearized, longitudinal equations of motion, including wind disturbances, assume the following standard form (refs. 1 to 4):

$$\dot{x} = Ax + Bu + Dw \tag{1}$$

where

$$x = \left(\theta \; u' \; \alpha \; q \; \frac{x - x_o}{U_o} \; \frac{z - z_o}{U_o} \; \delta T \; \delta th \; \delta s \; \delta e\right)^T$$

$$u = \left(\dot{\delta e} \; \dot{\delta s} \; \dot{\delta th} \; \dot{\delta}_{sp}\right)^T$$

and

$$w = \left(u'_w \; \alpha_w \; q_w\right)^T$$

where the states (x's) and the controls (u's) are

θ = perturbation in pitch angle,

u' = perturbation in velocity along x_s (stability) axis, normalized,

α = perturbation in angle of attack,

q = perturbation in the pitch rate,

$\frac{x - x_o}{U_o}$ = perturbation in the horizontal position of the aircraft (normalized),

$\frac{z - z_o}{U_o}$ = perturbation in the vertical position of the aircraft (normalized),

δT = perturbation in the thrust,

δth = perturbation in the throttle position,

δs = perturbation in stabilizer position,

δe = perturbation in the elevator position,

$\dot{\delta e}$ = perturbation in the elevator rate,

$\dot{\delta s}$ = perturbation in stabilizer rate,

$\dot{\delta th}$ = perturbation in throttle rate,

δsp = perturbation in spoiler position.

The subscript w indicates the perturbation in the variable due to wind disturbances. The model differs slightly from the previous studies (refs. 1 to 4) for reasons pointed out in section 1.

3.2. Wind Model

In order to complete and simulate the system model given by equation (1), the wind perturbation vector w must be specified. The components of this vector consist of u'_w, the normalized wind velocity in the + x_s direction*; α_w, the perturbation in the angle of attack due to the wind; and q_w, the

* This is a slight change in notation from previous reports (refs. 1, 3, and 4).

perturbation in the pitch rate of the aircraft due to wind. These wind variables may be logically modeled as the sum of a gust component with zero mean value and a steady component.

The gust components are modeled using the well-known Dryden spectrum (refs. 5, 6, 7). This method consists of using spectral factorization methods to obtain a dynamical system which generates a random process having the specified power spectral density when driven by white noise. Because of the linearity of the system, the three gust components can be treated individually; thus, only appropriate components are included in the longitudinal equations given in section 2.1. The detailed derivation of the gust components can be found in references 3 to 6 and will not be given here.

The Dryden spectra describe the statistical behavior of the wind gust velocities in the aircraft body-fixed coordinates, and the gust components can be expressed in the following form (refs. 3 to 7)

$$\dot{W}_g = A_{ww} W_g + B_{\xi_1} \xi_1 \tag{2}$$

where

$$W_g = (\alpha_{gb} \; \dot{\alpha}_{gb} \; q_{gb} \; u_{gb})^T$$

These four gust components constitute the four components (x_{11} to x_{14}) of the state vector. The elements of the matrices A_{ww} and B_{ξ_1} can be obtained from reference 3.

The steady-state components of the wind are simpler to model since they do not involve spectral factorization. These components can be modeled as the output of a first order deterministic plant, corrupted by a white noise. This can be done in different ways. One method, described in references 3 and 4, models the constant wind (or linearly varying wind) essentially as a white noise, with the known constant wind (or shear value) supplied as the initial condition. This method, although it seems to be working satisfactorily, has certain drawbacks. First, the system so modeled turns out to be uncontrollable. Thus, the constant feedback gains matrix cannot be computed for the complete system in the manner usually done for the regulator problems.

Reference 2 points out a method of computing the gains matrix in two parts by splitting the Riccati equation appropriately. The second drawback of this model is that it is only an approximate model for the following reason. Modeling the steady component of the wind merely as a white noise implies assumption of a constant time rate of change of a linear wind profile. Since the wind shear profiles are normally (and logically) given as spatial, rather than temporal profiles, the above assumption provides a linear shear with altitude only with a constant sink rate of the aircraft. This is not achieved either in the case when the aircraft is coming down on the flare path to touchdown (when the sink rate changes by an order of magnitude) or in the case when the aircraft is coming down on a glide slope with a nominal sink rate, but the wind velocity field is changing, thus introducing changes in the sink rate.

To permit modeling of spatial shears, a new method is proposed. The model also makes the whole system controllable, and the feedback gain matrix can be computed as is done in the usual manner for the regulator problems without the need for splitting the matrix Riccati equation in two.

Let the aircraft be coming down on a nominal glide slope in a steady flight condition. Also, for simplicity, let the aircraft be flying in a disturbance-free atmosphere for $\{t = s,\ s < 0\}$ (it is noted that the method can be trivially extended to the situation when the aircraft is flying in a constant wind for $\{t = s,\ s < 0\}$). Now, at $t = 0$, let the aircraft encounter a step wind, with a component U_{w_o} in $+ x_e$ direction and a component W_{w_o} in the $+ z_e$ direction. Also, let the subsequent wind field be described by a linear shear profile with a shear rate of X kn/30.48 m (100 ft) in the horizontal wind velocity, and Z kn/30.48 m (100 ft) in the vertical wind velocity. It is to be noted, in the present notation, that $U_{w_o} > 0$ represents a tailwind, $W_{w_o} > 0$ represents a downdraft, $X > 0$ represents a linear increase in tailwind (with decreasing height), and $Z > 0$ represents a linear increase in downdraft (with decreasing height) as seen by an earth-fixed observer.

If the inertial velocity of the aircraft is denoted by V_i and the flight path angle by γ°, then the sink rate of the aircraft is given by (fig. 1):

$$\dot{h} = -||V_i^I|| \sin \gamma \tag{3}$$

where superscript I denotes components are in inertial frame.

From this, the rate of change of wind velocity at the wing can be obtained as:

$$\dot{U}_w = -\frac{X}{100}||V_i^I|| \sin \gamma$$

$$= -\frac{X}{100}||V_i^I|| \sin \left\{\theta_o + \theta - (\alpha_o + \alpha_{s_i})\right\} \tag{4}$$

Expanding the right-hand side of the above equation, substituting

$$\gamma_o = \theta_o - \alpha_o \tag{5}$$

$$||V_i^I|| \sin \alpha_{s_i} = W_i^s = 0 + w_i^s \tag{6}$$

$$||V_i^I|| \cos \alpha_{s_i} = U_i^s = U_{i_o}^s + u_i^s \tag{7}$$

and simplifying yield

$$\dot{U}_w = -\frac{X}{100}\left[U_{i_o}^s \sin \gamma_o + U_{i_o}^s \cos \gamma_o \cdot \theta + \sin \gamma_o \cdot u - \cos \gamma_o \cdot w\right] \tag{8}$$

It is obvious that the first term in the above expression is the nominal rate of change of wind velocity and is included in the constant disturbance term W_d. Thus, the rate of change of the perturbation wind velocity in the horizontal direction (after normalizing with $U_{i_o}^s$) is given by

$$\dot{u}'_w = -\frac{X}{100}\left(\cos \gamma_o \cdot \theta + \sin \gamma_o \cdot u' - \cos \gamma_o \cdot \alpha\right) \tag{9}$$

Similarly, the rate of change of the normalized perturbation wind velocity in the vertical direction is given by

$$\dot{w}'_w = -\frac{Z}{100}\left(\cos\gamma_o \cdot \theta + \sin\gamma_o \cdot u' - \cos\gamma_o' \cdot \alpha\right) \tag{10}$$

Note that equations (8) and (9) yield the perturbation components of the wind at the wing. However, due to inertia effects, the flow field over the wing does not sense these changes until it travels about four chord lengths. These inertia effects can be modeled by a first order lag term with an appropriate time constant. Thus, the steady-state components of the perturbation wind velocity in a shear field can be modeled as

$$\begin{aligned}
\dot{x}_{15} &= -a_1 x_{15} + b_1 x_{17} \\
\dot{x}_{16} &= -a_1 x_{16} + b_1 x_{18} \\
\dot{x}_{17} &= -\frac{X}{100}\left(\cos\gamma_o \cdot \theta + \sin\gamma_o \cdot u' - \cos\gamma_o \cdot \alpha\right) \\
\dot{x}_{18} &= -\frac{Z}{100}\left(\cos\gamma_o \cdot \theta + \sin\gamma_o \cdot u' - \cos\gamma_o \cdot \alpha\right)
\end{aligned} \tag{11}$$

where

x_{15} = horizontal component of actual perturbation wind velocity felt by the wing, u'_{w_a}

x_{16} = vertical component of actual perturbation wind velocity felt by the wing, w'_{w_a}

x_{17} = horizontal component of perturbation wind velocity at the wing, u'_w, and

x_{18} = vertical component of perturbation wind velocity at the wing, w'_w.

The 4 steady-state wind variables can now be augmented with the 10 aircraft states [eq. (1)] and 4 gust components to yield the complete state variable model of the aircraft motion in the presence of atmospheric disturbance.

The system model as developed above is completely controllable in addition to being more realistic than the previous attempts to model the atmospheric disturbance effects. The optimal, constant feedback gain matrix for this system can now be computed in the usual way as for a regulator problem, with the two nominal shear components acting as constant disturbances on the system. The methods to compute the gain matrix are described in detail in section 4.

3.3. The Basic Augmented System: Aircraft in a Wind Disturbance Field

With the derivation of the wind model for steady wind velocity components now complete, it is possible to augment the wind model [eq. (11)] with the aircraft equations of motion in presence of wind disturbances [eq. (1)] to yield the state equations of the basic augmented system.

The final form of the wind model assumed the following form:

$$\dot{W}_g = A_{ww} W_g + B_{\xi_1} \xi_1 \tag{12}$$

$$\dot{W}_s = A_{wx} x + B_{\xi_2} \xi_2 + B_w W_d \tag{13}$$

where ξ's are white noise processes to account for the unknown disturbances and the wind vectors are

$$W_g = \left(\alpha_{gb} \; \dot{\alpha}_{gb} \; q_{gb} \; u'_{gb}\right)^T$$

and

$$W_s = \left(u'_w \; w'_w \; u'_{w_a} \; w'_{w_a}\right)^T$$

Here the subscripts g and s refer to gust and steady components respectively. The elements of the matrices A_{ww}, B_{ξ_1}, and B_{ξ_2} can be obtained from references 3 and 4. The elements of the A_{wx} and B_w can be obtained from equation (11).

Defining a composite wind vector

$$W \triangleq (W_g^T \; W_s^T)^T \tag{14}$$

the wind vector w defined in equation (1) can be expressed as

$$w = \begin{bmatrix} C_{wg} & C_{ws} \end{bmatrix} \begin{Bmatrix} W_g \\ W_s \end{Bmatrix} \tag{15}$$

where $[C_{wg} \; C_{ws}]$ is an appropriate transformation matrix (ref. 3). The steady winds, the wind shears, and the gusts can now be included in the system equation (1).

The complete system equations, with the inclusion of the wind model, can now be expressed in the standard state variable form as

$$\begin{Bmatrix} \dot{x} \\ \dot{W}_g \\ \dot{W}_s \end{Bmatrix} = \begin{bmatrix} A & DC_{wg} & DC_{ws} \\ 0 & A_{ww} & 0 \\ A_{wx} & 0 & 0 \end{bmatrix} \begin{Bmatrix} x \\ W_g \\ W_s \end{Bmatrix} + \begin{bmatrix} B \\ 0 \\ 0 \end{bmatrix} u + \begin{bmatrix} 0 \\ 0 \\ B_w \end{bmatrix} W_d + \begin{bmatrix} 0 & 0 \\ B_{\xi_1} & 0 \\ 0 & B_{\xi_2} \end{bmatrix} \begin{Bmatrix} \xi_1 \\ \xi_2 \end{Bmatrix}$$

or

$$\dot{\bar{x}} = \bar{A}\bar{x} + \bar{B}u + \bar{B}w + \bar{B}_w + W_d + \bar{B}_\xi \xi \tag{16}$$

The equations are now in a form suitable for applying the techniques of optimal control theory.

4. DERIVATION OF THE CONTROL LAWS

The equations of motion given by equation (16) represent the linear vector-matrix differential equations in state variable form governing the longitudinal motion of the aircraft in the presence of atmospheric disturbances. These (continuous-time) differential equations are now expressed in a discrete form which updates the state variables from one sampling instant to

the next. The discretization of the state equations is desirable for various reasons. One, the system equations are integrated on a digital computer and, so, are inherently discrete in nature. Secondly, the aircraft control system also utilizes a digital computer to perform the implementation of the desired control law derived. Also, the measurement data obtained from the MLS (Microwave Landing System) is provided at discrete intervals of time, rather than in a continuous fashion. Thus, it will be easier at a later stage to cascade the discrete controller obtained here with a discrete estimator.

The differential equation (16) can be expressed in a discretized form using a standard procedure [refs. 3, 4, 8] as follows:

$$\bar{x}\big((k+1)T\big) = F(T)\,\bar{x}(kT) + G(T)\,u(kT),\quad k = 0,1,2\ldots,(k_f - 1) \tag{17}$$

where

$$\bar{x} = \begin{Bmatrix} x \\ w \end{Bmatrix},\quad F(T) = e^{\bar{A}T}$$

$$G(T) = \left(\int_0^T e^{\bar{A}\tau}\, d\tau\right)\bar{B}$$

with T = sample time interval.

The optimal control law for the above discrete linear system is now developed for the following cases:

(1) the disturbance-free system — the linear regulator problem, and

(2) the system in wind disturbance — the linear regulator with constant disturbance (input) problem for the:

   (a) output integral feedback case, and
   (b) control derivative constraint case.

The basic optimal constant-gain, feedback control law for the regulator problem is derived using a nonrecursive solution of the Riccati equation. The method of solution (refs. 9 to 11) is outlined in some detail in section 4.1. The same method is used to compute the feedback gain matrix for the system with the constant disturbance problem, after augmenting the original system appropriately. These modifications are outlined in sections 4.2. and 4.3.

4.1. The Linear Regulator Problem

In this section, the basic, optimal, constant gain, feedback control law is derived for a disturbance-free linear regulator problem using a nonrecursive solution of the Riccati equation. The method is described in complete detail in references 9, 10, and 11. The method is used here to derive the constant gain control law to execute an optimal flare maneuver in the absence of any atmospheric disturbances. The method yields a discrete, constant gain law to implement the optimal, state-estimate, feedback control law. The method is outlined briefly in this section for the sake of completeness.

The deterministic, linearized, longitudinal equations of motion of the aircraft flying in a disturbance-free atmosphere can be written in the following form

$$\dot{x} = Ax + Bu \qquad x(o) = x_o \qquad o \leq t \leq t_f \tag{18}$$

where

$$x = \left(\theta \; u' \; \alpha \; q \; \frac{x - x_o}{U_o} \; \frac{z - z_o}{U_o} \; \delta T \; \delta th \; \delta s \; \delta e\right)^T$$

and

$$u = \left(\dot{\delta e} \; \dot{\delta s} \; \dot{\delta th} \; \dot{\delta sp}\right)^T$$

The complete description of the aircraft states (x's) and controls (u's) was given in section 3.1. It is noted that the above equations are obtained from equation (1) just by omitting the wind disturbance part. These equations can be expressed in discrete form as

$$x_{k+1} = Fx_k + Gu_k, \; x(o) = x_0, \; k = 0, \; 1, \; 2, \ldots k_{f-1} \tag{19}$$

The quadratic performance index to be minimized for the above discrete system can be expressed as

$$J = \frac{1}{2} x_f^T Q_f x_f + \frac{1}{2} \sum_{k=0}^{k_{f-1}} \left(x_k^T Q x_k + u_k^T R u_k\right) \tag{20}$$

where the penalty matrices Q_f, Q, and R are assumed to be constant. Forming the Hamiltonian for the problem in the usual way, one can easily write the adjoint vector equation for the Lagrangian multiplier λ canonical backward difference equation form (ref. 12):

$$\lambda_k = Qx_k + F^T\lambda_{k+1} \tag{21}$$

$$\lambda_{k_f} = Q_f x_{k_f} \tag{22}$$

From the maximum principle, the optimal control is given by

$$u_k = - R^{-1}G^T\lambda_{k+1} \tag{23}$$

Rearranging and combining the state vector and the adjoint vector equations yield the following canonical backward difference equation

$$\begin{Bmatrix} x_k \\ \lambda_k \end{Bmatrix} = \begin{bmatrix} F^{-1} & F^{-1}GR^{-1}G^T \\ QF^{-1} & (F^T + QF^{-1}GR^{-1}G^T) \end{bmatrix} \begin{Bmatrix} x_{k+1} \\ \lambda_{k+1} \end{Bmatrix} \triangleq \begin{bmatrix} H_c \end{bmatrix} \begin{Bmatrix} x_{k+1} \\ \lambda_{k+1} \end{Bmatrix} \tag{24}$$

with a set of split boundary conditions,

$$x(0) = x_o \quad \text{and} \quad \lambda_{k_f} = Q_f x_f \tag{25}$$

Assuming the solution of λ_k of the form

$$\lambda_k = P_k x_k, \quad P_{k_f} = Q_f \tag{26}$$

a recursive solution can be obtained for P_k in the usual way (ref. 12). However, a nonrecursive solution of P can be computed in the following way, which is very useful, especially for the infinite-time, constant gain solution desired in the present study. The details of the method can be obtained in references 9, 10, and 11.

If W is the eigenvector matrix corresponding to the eigenvalues of the canonical system matrix H_c as defined above, and further if

$$W = \begin{bmatrix} W_{11} & W_{12} \\ W_{21} & W_{22} \end{bmatrix} \tag{27}$$

then the steady-state solution of P is given by

$$P_\infty = W_{21} W_{11}^{-1} \tag{28}$$

The optimal control law is then obtained as

$$u_k = - R^{-1} G^T \left[P_\infty^{-1} + G R^{-1} G^T \right]^{-1} F x_k \tag{29}$$

The closed-loop, constant gain, state-estimate, feedback control law derived above can now be implemented easily by solving the physical system forward in time.

4.2. The Regulator Problem: Constant Disturbance Case

The basic disturbance-free system discussed in the last section can now be extended to include the wind model described in section 3.2. in order to study the flight performance of the aircraft flying in atmospheric disturbances.

As pointed out in section 3, the linearized, longitudinal equations of motion, including the wind disturbances, assume the following form [eq. (16)]:

$$\dot{\bar{x}} = \bar{A}\,\bar{x} + \bar{B}\,u + \bar{B}_w W_d + \bar{B}_\xi\,\bar{\xi} \tag{30}$$

These continuous-time, differential equations can be again put in discrete form as

$$\bar{x}_{k+1} = \bar{F}\,\bar{x}_k + \bar{G} u_k + \bar{G}_w W_d + \bar{G}_\xi\,\bar{\xi}_k \tag{31}$$

As was pointed out in section 3.2, the pair $[\bar{F},\bar{G}]$ for the above system is controllable; hence, the constant, feedback gain matrix can be computed in the

usual way. However, the presence of the constant disturbance vector W_d (the two shear values X, Z, see section 3.2) necessitates a slight modification of the above system equations. This modification can be done in two different ways. One way would be to augment the above system for implementing integral feedback of some of the variables. The second method is to constrain the control derivatives by augmenting the control variables with the above system equations. The methods of deriving the desired control law in both cases are explained in detail in the following sections, which point out their advantages and disadvantages respectively.

4.2.1. Integral feedback case. — One method to eliminate the effect of constant disturbances acting on the system is application of the integral feedback law. The details of the method can be found in reference 13. The method is briefly outlined below.

Let the deterministic system be described by the discrete difference equations

$$x_{k+1} = Fx_k + Gu_k + W_o, \qquad x(0) = x_o \tag{32}$$

where W_o is the constant disturbance acting on the plant. Let the controlled variables by given by

$$z_k = Dx_k \tag{33}$$

Adding to the system variables the integral state defined by

$$q_{k+1} = q_k + z_k, \qquad q(0) = q_o \tag{34}$$

and augmenting this integral state variable with the original system, it can be shown that a time-invariant control law of the form

$$u_k = H_{11}x_k + H_{12}q_k \tag{35}$$

is an asymptotically stable control law such that the effects of the constant disturbances on the controlled variables eventually vanish. It can also be

shown that the necessary and sufficient conditions for the existence of the above control law are that: (1) the original system be stabilizable; and (2) the open-loop transfer matrix has no zeroes at the origin.

The above conditions impose certain restrictions on the choice of the controlled variables. After a few trials, the following variables were selected as the controlled variables for the integral feedback scheme (note that the following are perturbations):

$$
\begin{aligned}
z_1 &= \theta - \alpha & \dot{q}_1 &= z_1 \\
z_2 &= u' & \dot{q}_2 &= z_2 \\
z_3 &= \dot{h} & \dot{q}_3 &= z_3 \\
z_4 &= \frac{x - x_o}{U_o} & \dot{q}_4 &= z_4
\end{aligned}
\tag{36}
$$

The integral state variables can now be augmented with the system equations of motion with wind disturbance input, derived in section 3.3, and the complete system can be expressed as

$$
\begin{Bmatrix} \dot{\bar{x}} \\ \dot{q} \end{Bmatrix} = \begin{bmatrix} \bar{A} & 0 \\ A_q & 0 \end{bmatrix} \begin{Bmatrix} \bar{x} \\ q \end{Bmatrix} + \begin{bmatrix} \bar{B} \\ 0 \end{bmatrix} u + \begin{bmatrix} \bar{B}w \\ 0 \end{bmatrix} W_d \tag{37}
$$

These equations can be discretized in the usual way. The optimal control problem can then be solved by computing the constant gain matrix using the same method described in section 4.1.

The optimal, closed-loop time response of the aircraft flying in a given wind disturbance can then be obtained by solving the following sets of discrete difference equations:

$$
\begin{aligned}
\bar{x}_{k+1} &= \bar{F}\,\bar{x}_k + \bar{G}(H_{11}\bar{x}_k + H_{12}q_k) + \bar{G}_w W_d \\
q_{k+1} &= F_1 q_k + F_2 \bar{x}_k
\end{aligned}
\tag{38}
$$

The results of the simulation of this closed-loop system are presented in section 4.

4.2.2. Control Derivative Constraint Case. — A second method to eliminate the effects of the constant disturbance acting on the system is by application of the regulator problem with constraints imposed on the control variable derivatives. This is achieved by penalizing the derivative of the control variable in the performance index and augmenting the original system by defining the control variable as additional state. The details of the method can be found in reference 14 for the case of continuous systems. The derivation of the control law for the discrete systems differs slightly from that for the continuous case and is given in some detail below.

Let the original system be described by the discrete equations

$$x_{k+1} = Fx_k + Gu_k + G_w W_d, \qquad x(0) = x_o \tag{39}$$

where W_d is the constant disturbance acting on the system. Now, to achieve the desired objective of driving the state x and its derivative $\dot{x}$ to zero (asymptotically), the following condition must be satisfied

$$Gu_k = - G_w W_{d_k} \qquad \text{as } k \to \infty \tag{40}$$

This implies that the range space of G_w is contained in the range space of G. The system equations can then be written as

$$x_{k+1} = Fx_k + G(u_k + W) \tag{41}$$

where

$$W = (G^T G)^{-1} G^T G_w W_d \tag{42}$$

Defining a new control variable

$$u_{1_k} = (u_k + W), \qquad u_{2_k} = \dot{u}_{1_k} \tag{43}$$

and noting that

$$\dot{W} = 0$$

a performance index can be defined for the above problem, with the derivative constraint on the control included, as follows

$$J = \frac{1}{2} \sum_{k=1}^{\infty} \left\{ x_k^T Q x_k + (u_k + W)^T R(u_k + W) + u_{2_k}^T S\, u_{2_k} \right\} \tag{44}$$

for the augmented system

$$\begin{Bmatrix} x_{k+1} \\ u_{1_{k+1}} \end{Bmatrix} = \begin{bmatrix} F & G \\ F_{11} & F_{12} \end{bmatrix} \begin{Bmatrix} x_k \\ u_{1_k} \end{Bmatrix} + \begin{bmatrix} 0 \\ G_{12} \end{bmatrix} u_{2_k} \tag{45}$$

The optimal control law for this system can now be computed in the same manner as before (section 4.1) and is obtained as

$$\begin{aligned} u_{2_k} &= H_{11} x_k + H_{12} u_{1_k} \\ &= H_{11} x_k + H_{12}(u_k + W) \end{aligned} \tag{46}$$

Substituting for u_{2_k} as

$$u_{2_k} = \frac{u_{k+1} - u_k}{\Delta T}, \qquad \Delta T = \text{time interval}$$

$$u_{k+1} = H_{11} x_k\, \Delta T + (H_{12}\, \Delta T + I) u_k + H_{12} W\, \Delta T, \qquad u(0) = 0 \tag{47}$$

Substituting this control law, the original system equations can now be solved by simulation on a digital computer as usual.

It is easily seen that the feedback law requires a priori knowledge of the magnitude of the constant disturbance acting on the system. In practice, this knowledge cannot always be expected, which is a potential disadvantage of the method. In the cases simulated in the present study, the a priori knowledge of the magnitude of the disturbance was assumed. In these cases, it is observed that the performance of the system was much better than with the integral feedback case discussed in section 4.2.1.

5. RESULTS

With the development of the system model, both for the wind-disturbance-free case and for the wind-disturbance case, outlined in section 3, and the development of the various digital control laws for these systems derived in section 4, it is now possible to simulate the system equations of motion with the constant gain, closed-loop, optimal control law included to evaluate the flight performance of the system. The general approach to study the flare performance is similar to the one in previous studies (refs. 1 and 2). Thus, the longitudinal equations of motion of the aircraft are expressed in linearized form about the desired touchdown trajectory. These equations are then discretized; the appropriate control law is incorporated into the system equation, and the system is expressed as a closed-loop system. The difference between the initial glide slope and the desired touchdown conditions (table 1) is supplied as an initial condition, and the time response of the closed-loop system is simulated on a digital computer.

The results obtained by formulating the flare problem in the above manner show that, initially, the sink rate increases before being reduced to the desired touchdown value. This increase, though small and probably tolerable, was noted consistently in both the cases: with time-varying gain in previous study (ref. 1) and with the constant gain in the present study. This was considered undesirable from the viewpoint of pilot monitoring as well as passenger comfort. Hence, it was also decided to conduct a preliminary study with an open-loop control law forced on the system. A few simple forms of control law (linearly varying or ramps) were selected to study the performance in the absence of any disturbance. In all the cases, the elevator and the throttle were prevented from assuming negative values.

Figures 2a to 2c show the time response of an optimal transition from a -3° glidepath to the desired touchdown corditions in the absence of any wind disturbances. Figure 2a shows the time history of altitude h, the sink rate $\dot{h}$, and the normalized horizontal tracking error $(x-x_o)/U_o$ from the nominal path. It is seen that at 7.1 sec, when the simulation was terminated, the aircraft had a sink rate of 0.5452 m/sec (1.798 ft/sec) and a horizontal error of 5.87 m (19.26 ft). The aircraft is still 0.21 m (0.6872 ft) above ground and will have touchdown at approximately 7.5 sec. The pitch and pitch rate histories are shown in figure 2b. The maximum pitch rate is about 2.87°/sec, which is acceptable. Figure 2c shows the thrust and the throttle history. The thrust has been reduced to about 9340 N (2100 lbs) at 7.1 sec. It is noted, however, that the throttle rate is a little too high. This could be corrected by increasing the appropriate penalty term, albeit with a resulting modification of the performance of other variables.

Figures 3a to 3c show the optimal transition from a -6° glide slope to the desired touchdown condition, again in the absence of wind disturbances. Figure 3a indicated that touchdown occurs at 5.1 sec with the sink rate at touchdown being 0.698 m/sec (2.29 ft/sec) and the horizontal tracking error about 9.14 m (30 ft). Figure 3b shows the time history of pitch and pitch rate. The maximum pitch rate is about 3.3°/sec, which is acceptable. Figure 3c shows the time histories of the thrust and the throttle. The magnitude of the thrust at touchdown is 9518.7 N (2140 lbs), which is slightly above the idle thrust required.

Figures 4 to 9 show the flight performances of the aircraft in the presence of wind disturbance with specified shear profiles. Figures 4 to 8 show the performance of the aircraft when it is trying to track the -3° glide slope in the presence of gust and wind disturbances with specified shear profiles. Figure 9 shows the time response of optimal transition from a -3° glidepath to desired touchdown conditions.

Figure 4 shows the time response of an aircraft, initially on a -3° glidepath, trying to track the path when it encounters a 10-kn headwind decreasing at 5 kn/30.48 m (100 ft) and a 5-kn updraft decreasing at 1 kn/30.48 m (100 ft). The control law used here is the one derived in section 4.2.1 (integral feedback law). It is seen from figure 4a that the sink rate shows

an oscillatory behavior and at 7.1 sec shows a value of 3.91 m/sec (12.86 ft /sec), which is higher than the nominal value of 3.37 m/sec (11.07 ft/sec). Figure 4b shows the pitch and pitch rate history, and the maximum pitch rate is about -2.92°/sec, which is within limits. Because of the higher lift available from a favorable wind field (headwind and updraft), reduced thrust and throttle settings were required to maintain the flight path, and this is reflected in figure 4c. The components of the wind velocity, both those at wing (u_w, w_w) and those actually felt by the wing (u_{wa}, w_{wa}), are plotted in figure 4d. As was noted in the derivation of the wind model (section 3.2) the actual velocities felt by the wing (which determine the aerodynamic lift and moments developed by the wing) lag the inertially changing components.

The effect of using the control law with the control derivative constraint (section 4.2.2), for tracking the glide slope under a wind profile identical to the above, is seen in figures 5a to 5c. It is clearly seen that the oscillatory behavior of the sink rate has been eliminated. Also, the sink rate at 7.1 sec is 3.52 m/sec (11.55 ft/sec), which is almost equal to the nominal sink rate, 3.37 m/sec (11.07 ft/sec). A comparison of figure 5b with figure 4b shows that the pitch and pitch rate histories are almost identical. Figure 5c shows that the throttle and thrust settings have been lowered only slightly compared to figure 4c.

Figures 6a to 6c show the interesting results achieved when the simulation was conducted without augmenting the original system with either integral state or the control variables. The appropriate gain matrix was computed and the system was simulated with the same wind profile (fig. 4d) acting on the aircraft. The time responses of figures 4a, 4b, and 4c look very similar to those of figures 6a to 6c, except for slightly higher thrust settings.

Figures 7a to 7c show the flight performance of the aircraft on a -3° glidepath entering a wind field shown in figure 7d. The aircraft encounters a 10-kn tailwind decreasing at 5 kn/30.48 m (100 ft) and a 5-kn updraft decreasing at 1 kn/30.48 m (100 ft). Figures 7a to 7c show the time histories of the various states. It is seen that the increased angle of attack (due to updraft) affects the performance faster than the decreasing airspeed (due to tailwind), and the sink rate begins to decrease initially.

Figures 8a to 8c show the performance of an aircraft entering a wind field shown in figure 8d. The aircraft encounters a tailwind at 10 kn

increasing at 5 kn/30.48 m (100 ft) and a downdraft of 5 kn increasing at 1 kn/30.48 m (100 ft). This is the most unfavorable wind profile simulated in the present study. Figures 8a to 8c show the time response of the closed-loop system using the control law with the control variable constraint method of section 4.2.2. The performance of the aircraft is seen to be satisfactory in the presence of an unfavorable wind profile. Again, the absence of any oscillatory behavior in the sink rate is noted.

Thus, it is noted that the performance of the closed-loop system is very much satisfactory when the aircraft is nominally on the glidepath and encounters a specified wind profile. The method was extended, as in the previous study (refs. 1, 2), to achieve an optimal transition from a nominal glide slope to the desired touchdown conditions, using the same set of optimal gains derived for the case having an identical wind profile. The differences between the desired touchdown trajectory and the nominal glide slope were supplied as the initial conditions to the problem, in addition to the specified wind conditions. However, it was found that in almost all cases the response tends to oscillate without achieving the touchdown conditions in the time interval considered. This is found to be mainly because of the large initial conditions and the resulting high corrections. However, one case was found to be working. Figure 9 shows the results of the simulation for this particular case. The aircraft is trying to achieve an optimum transition from a -3° glide slope to the desired touchdown conditions. The control law used here is derived for an unaugmented system, and the aircraft encounters a 10-kn headwind decreasing at 5 kn/30.48 m (100 ft), and a 5-kn updraft decreasing at 1 kn/30.48 m (100 ft). The aircraft touches down at 7.1 sec with a sink rate of about 0.249 m/sec (0.82 ft/sec). It is interesting to note here that, in spite of the favorable wind field (headwind and updraft), the sink rate increases slightly before being reduced to a low acceptable value for touchdown. This is in sharp contrast to figures 4 to 6 where the sink rate decreased under wind conditions identical to those assumed in the present case. Therefore, this result, together with results obtained in figures 2a, 3a, and in the previous study with time varying gains (ref. 1), clearly indicates a consistent trend in the sink rate history. The negative pitch and pitch rate (even though of very small magnitude) are, however, not acceptable in practice.

It was also decided to conduct some simulation runs with a few simple, open-loop control laws forced on the system and to observe the time responses of the aircraft. The open-loop law used for flare maneuver consisted of two ramps on the throttle and the elevator. Both were reduced from their nominal values to zero with varying rates and held at zero. Figures 9 and 10 show two sample runs.

Figure 10 shows the transition of the aircraft on a -3° glide slope to touchdown. The elevator rate imposed was 1.8 times the nominal rate, and the throttle rate was 2.9 times the nominal rate. The nominal rate is defined here as the rate which will reduce the control from its nominal initial value to zero in 7.1 sec. It is seen that the aircraft touches down at 6.8 sec with a sink rate of 0.289 m/sec (0.95 ft/sec). The maximum pitch rate was about 1.1°/sec. The discontinuities seen in the pitch rate history at 2.6 sec and 4.1 sec were due to the abrupt changes in the throttle rate and the elevator rate, respectively, at these instants in order to hold them at zero and prevent them from assuming negative values.

Figure 11 shows the flight performance of the aircraft trying to achieve a forced transition from a -6° glidepath to touchdown. The elevator rate imposed was 3.1 times the nominal rate, and the throttle rate was 2.9 times the nominal rate (defined above). The performance was very similar to the previous case, except for a higher maximum pitch rate (2.3°/sec) due to a higher elevator rate.

It is to be noted that the simulated studies with open-loop control law showed that the performance of the aircraft was very sensitive to the small changes in the control variable (rates). For example, in the -6° glidepath case shown above, keeping the throttle rate at 2.9 (times the nominal rate), simulation runs were conducted at different elevator rates. It was found that an elevator rate of 3.0 resulted in an early and unacceptably hard landing (touchdown at 5.6 sec at sink rate of 1 m/sec), whereas an elevator rate of 3.25 results in no touchdown, with aircraft actually climbing before 7.1 sec. Results obtained for a -3° glide slope also showed similar behavior of extreme sensitivity to small control variations. This behavior was considered unacceptable, and hence the open-loop control law should be implemented as a nominal law to be supplemented by a closed-loop control law derived in any one of the several ways available.

6. CONCLUSIONS

A discrete, time-invariant, optimal, closed-loop control law was presented for a linear regulator problem. The method was extended to include a system being acted upon by a constant disturbance. Two forms of control laws were derived to solve this problem. One method utilized the feedback of integral states defined appropriately and augmented with the original system equations. The second method formulated the problem as a control variable constraint, and the control variables were augmented with the original system.

A new method of formulating the wind model was described. It was shown that the new wind model was more realistic than the previous model which modeled the steady, shearing winds as a white noise with known initial conditions. The present wind model also overcame the uncontrollability problem posed by the previous model, and it was shown that the optimal gains could be computed in the same way as for a regulator problem with a constant disturbance acting on the system.

The various control laws derived were implemented to simulate the closed-loop system in following cases:

(1) optimal flare transition from glide slope to touchdown in absence of winds,

(2) glide slope tracking in presence of various wind profiles specified,

(3) optimal flare transition in presence of wind profiles specified, and

(4) flare with open-loop control laws forced on the system.

It was shown that the flight performance of the aircraft was satisfactory and within acceptable limits in cases (1) and (2).

It was seen that the optimal gains computed for case (3) failed to achieve an optimal transition from glide slope to touchdown in presence of wind disturbances, even though the same gains performed satisfactorily in case (2). It was pointed out that this is due to the large initial conditions (errors) imposed, which force overcorrections. Only one simulation result was presented for this case. It is proposed to conduct further study of this case by passing the large initial error through a low-pass filter and using the output of this filter as a feedback variable initially.

It was also shown that the control variable constraint control law yields a better performance compared to feedback control law for the integral states chosen. However, as was pointed out, the previous method requires a priori knowledge of the magnitude of the disturbance acting on the system.

In the study with open-loop control laws forced on the system to achieve the flare maneuver (case 4), it was shown that, although this law was extremely desirable, the performance is very sensitive to small variations in controls even in absence of winds. It is therefore proposed to reformulate the problem as a tracking problem, with the open-loop control law obtained experimentally, as a baseline law, supplemented by a closed-loop, optimal gain, feedback control law.

REFERENCES

1. Nadkarni, A.A.: Digital Flare Law Development. Final Report, NASA contract NAS1-14193-34, Dec. 1977.

2. Nadkarni, A.A.: Comparative Study of Flare Control Laws. Progress Report, NASA Grant NSG 1480, July 1978.

3. Halyo, N.: Development of an Optimal Automatic Control Law and Filter Algorithm for Steep Glide Slope Capture and Glideslope Tracking. NASA CR-2720, Aug. 1976.

4. Halyo, N.: Development of a Digital Automatic Control Law for Steep Glideslope Capture and Flare. NASA CR-2834, June 1977.

5. Etkin, B.: Dynamics of Atmospheric Flight. John Wiley and Sons, Inc., 1972.

6. Roskam, J.: Flight Dynamics of Rigid and Elastic Airplanes. Roskam Aviation and Engineering Corporation, Kansas, 1972.

7. McRuer, D.; Ashkenas, I.; and Graham, D.: Aircraft Dynamics and Automatic Control. Princeton University Press (Princeton, NJ), 1973.

8. Ogata, K.: State Space Analysis of Control Systems. Prentice-Hall, Inc., 1967.

9. Vaughan, D.R.: A Nonrecursive Algebraic Solution for the Discrete Riccati Equation. IEEE Trans. AC, Oct. 1970, pp. 597-599.

10. Vaughan, D.R.: A Negative Exponential Solution for the Linear Optimal Regulator Problem. Proc. JACC, 1968.

11. Vaughan, D.R.: A Negative Exponential Solution to the Matrix Riccati Equation. IEEE Trans. AC-14, Feb. 1969, pp. 72-75.

12. Sage, A.P.: Optimum Systems Control. Prentice-Hall, Inc., 1968.

13. Kwakernaak, H.; and Sivan, R.: Linear Optimal Control Systems. John Wiley and Sons, Inc., 1972.

14. Anderson, B.D.O.; and Moore, J.B.: Linear Optimal Control. Prentice-Hall, Inc., 1971.

Table 1. Desired terminal (or touchdown) conditions.

Parameter	Values
θ	3°
u'	0.0
α	3.52°
g	0°/sec
$\frac{x - x_o}{U_o}$	—(not constrained)
$\frac{z - z_o}{U_o}$	0
thrust	idle thrust = 8896 N
throttle	0°

Table 2. Inertial wind profiles simulated.

Profile	Wind Parameter
A	Head wind of 10 kn decreasing at 5 kn/30.48 m
	Updraft of 5 kn decreasing at 1 kn/30.48 m
B	Tailwind of 10 kn decreasing at 5 kn/30.48 m
	Updraft of 5 kn decreasing at 1 kn/30.48 m
C	Tailwind of 10 kn increasing at 5 kn/30.48 m
	Downdraft of 5 kn increasing at 1 kn/30.48 m

Table 3. Types of controllers simulated.

Type	Description
1	Linear regulator case (no wind)
2A	Linear regulator with constant disturbance — integral feedback case
2B	Linear regulator with constant disturbance — control derivative constraint case
2F	Linear regulator with constant disturbance — unaugmented system
3	Open-loop — forced input case (no wind)

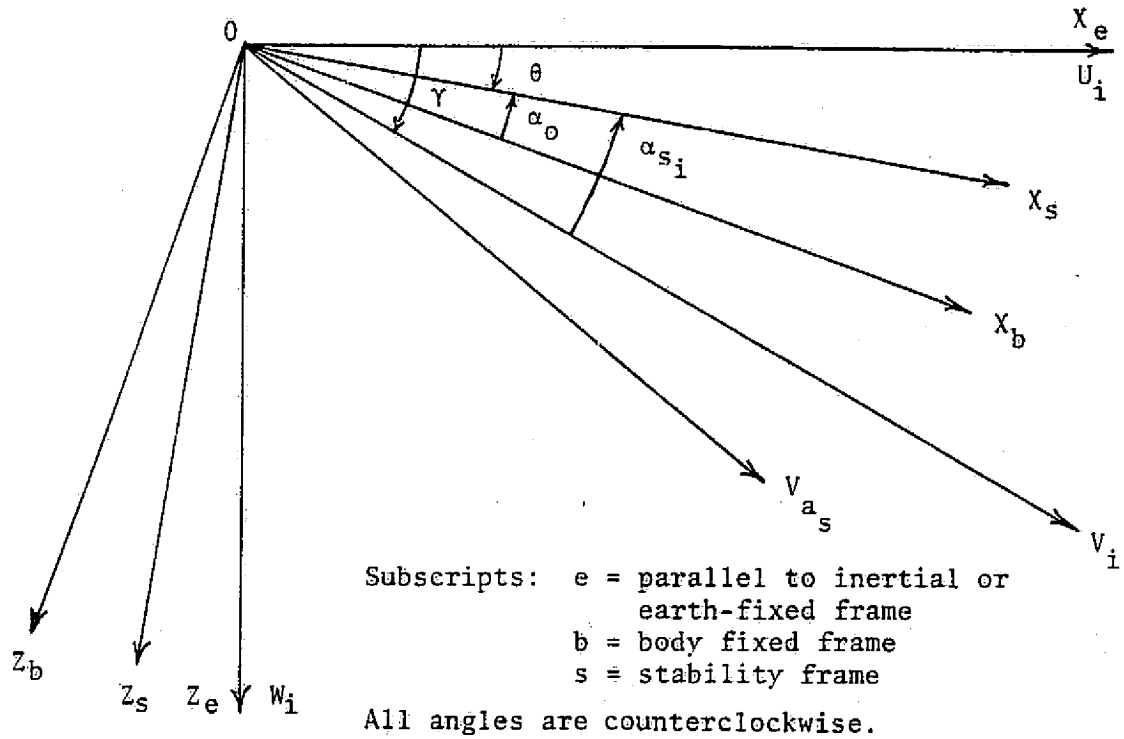

Figure 1. Coordinate frame and flight geometry.

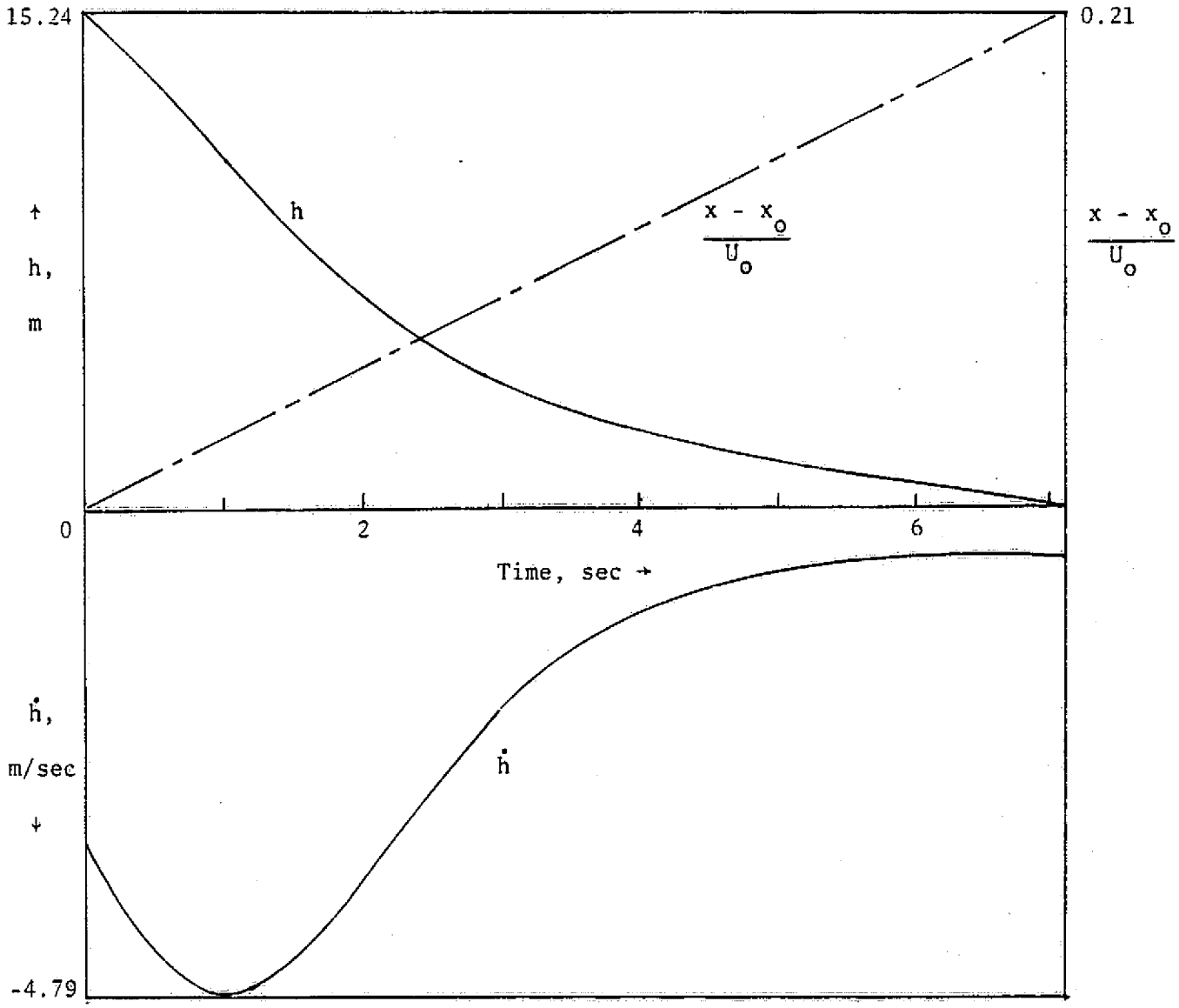

Figure 2(a). Flare response, -3° glide slope: altitude, sink rate, and horizontal dispersion; no wind case, controller 1.

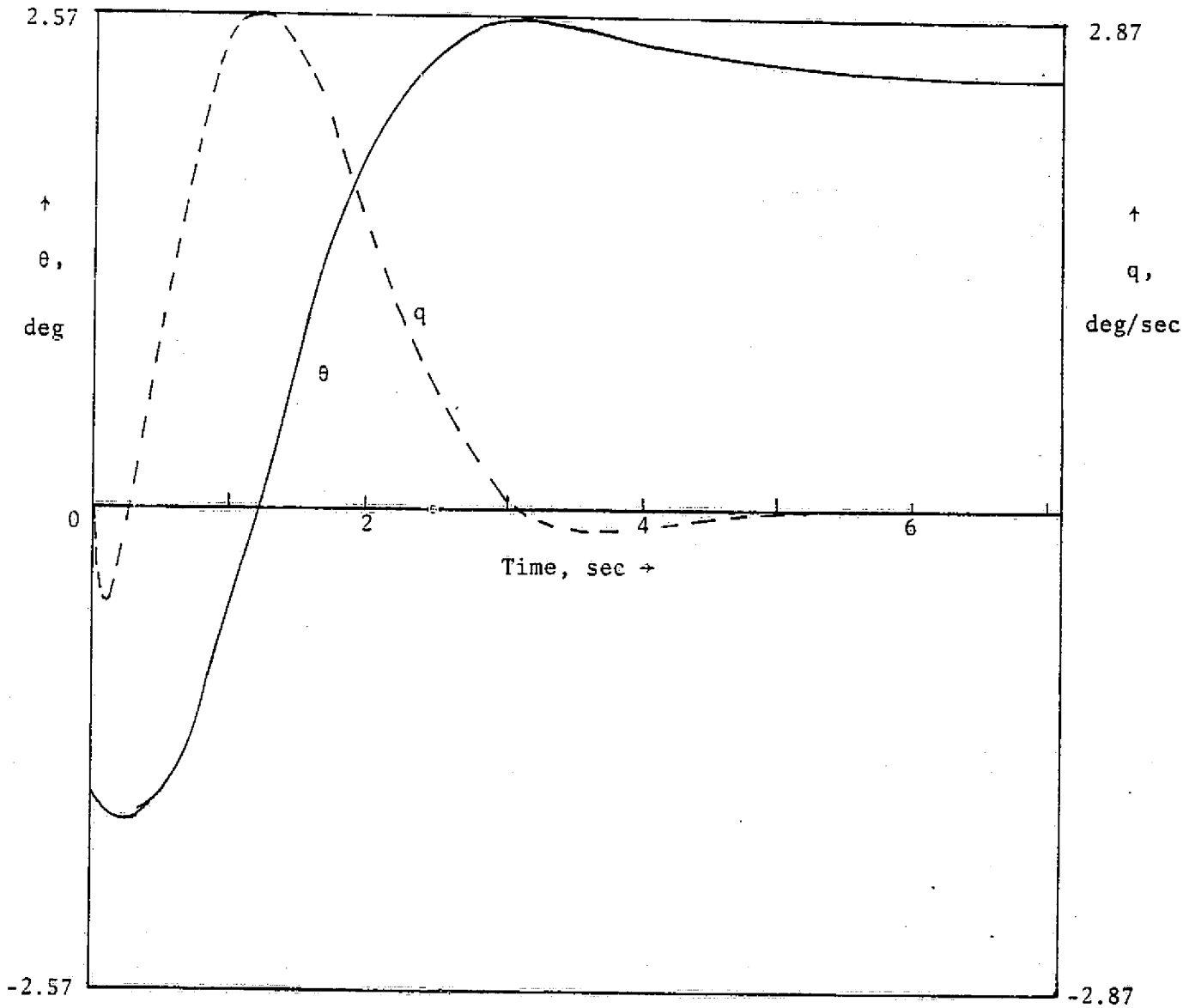

Figure 2(b). Flare response, -3° glide slope: pitch and pitch rate; no wind case, controller 1.

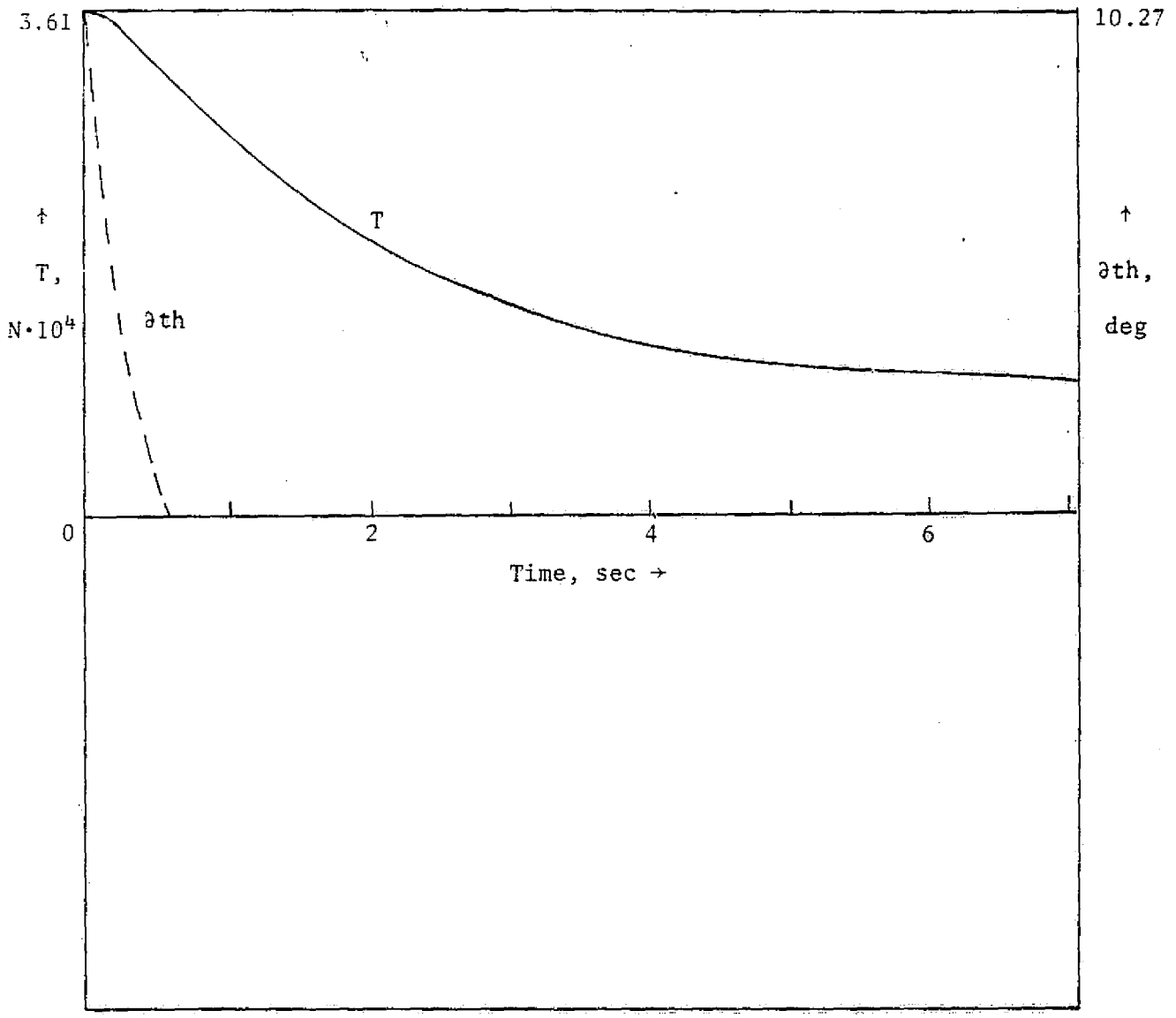

Figure 2(c). Flare response, -3° glide slope: thrust and throttle; no wind case, controller 1.

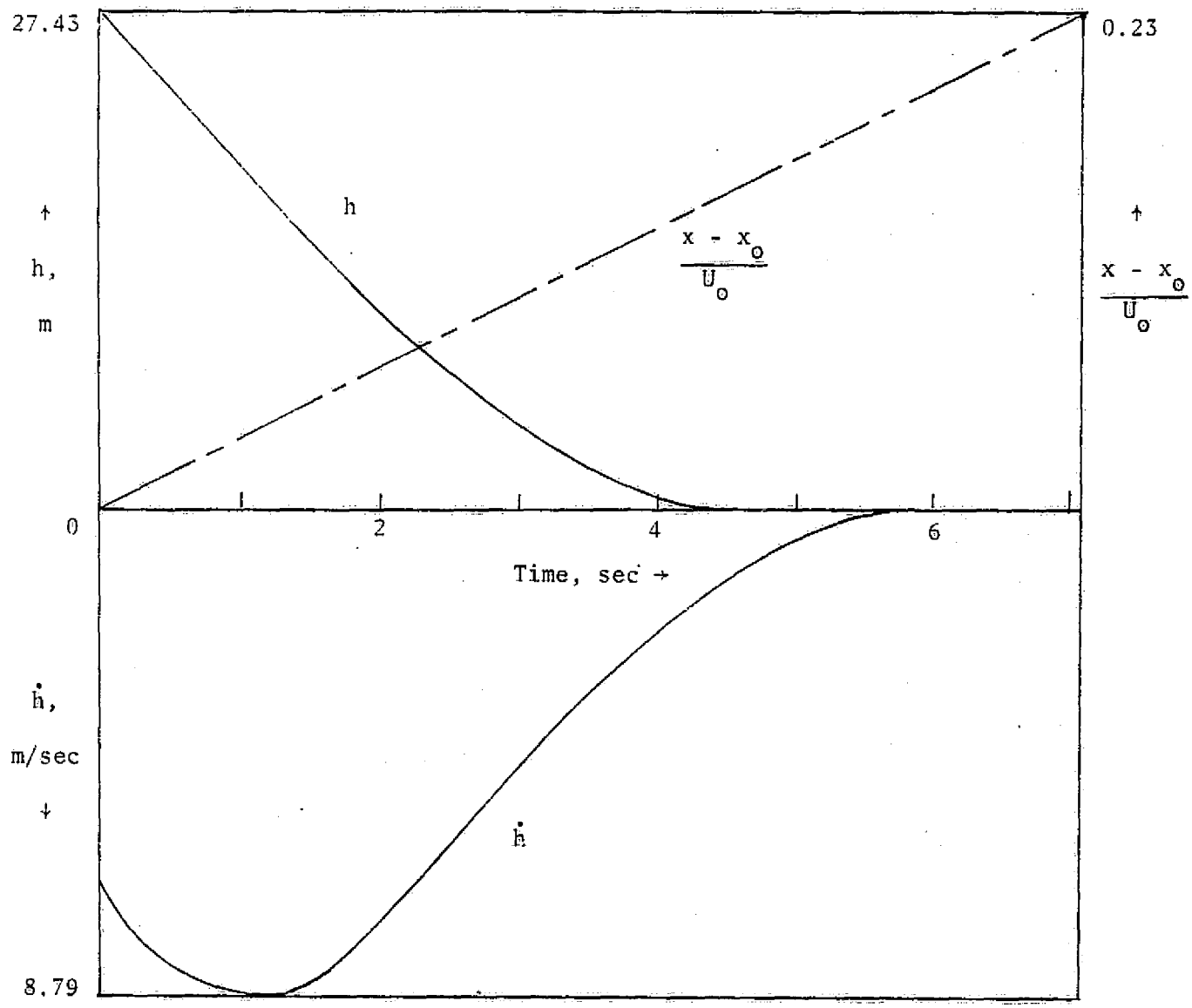

Figure 3(a). Flare response, -6° glide slope: altitude, sink rate, and horizontal dispersion; no wind case, controller 1.

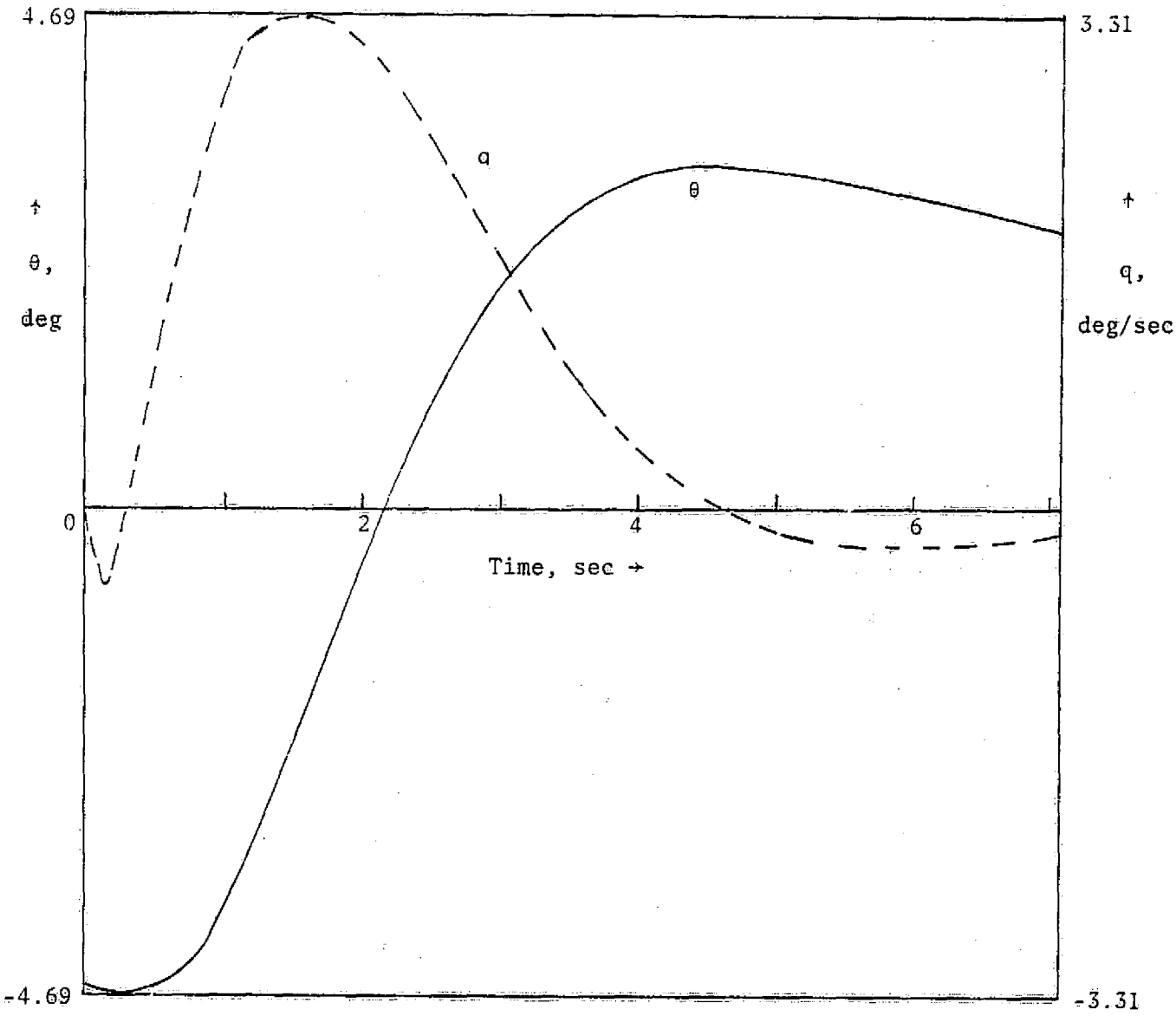

Figure 3(b). Flare response, -6° glide slope: pitch and pitch rate; no wind case, controller 1.

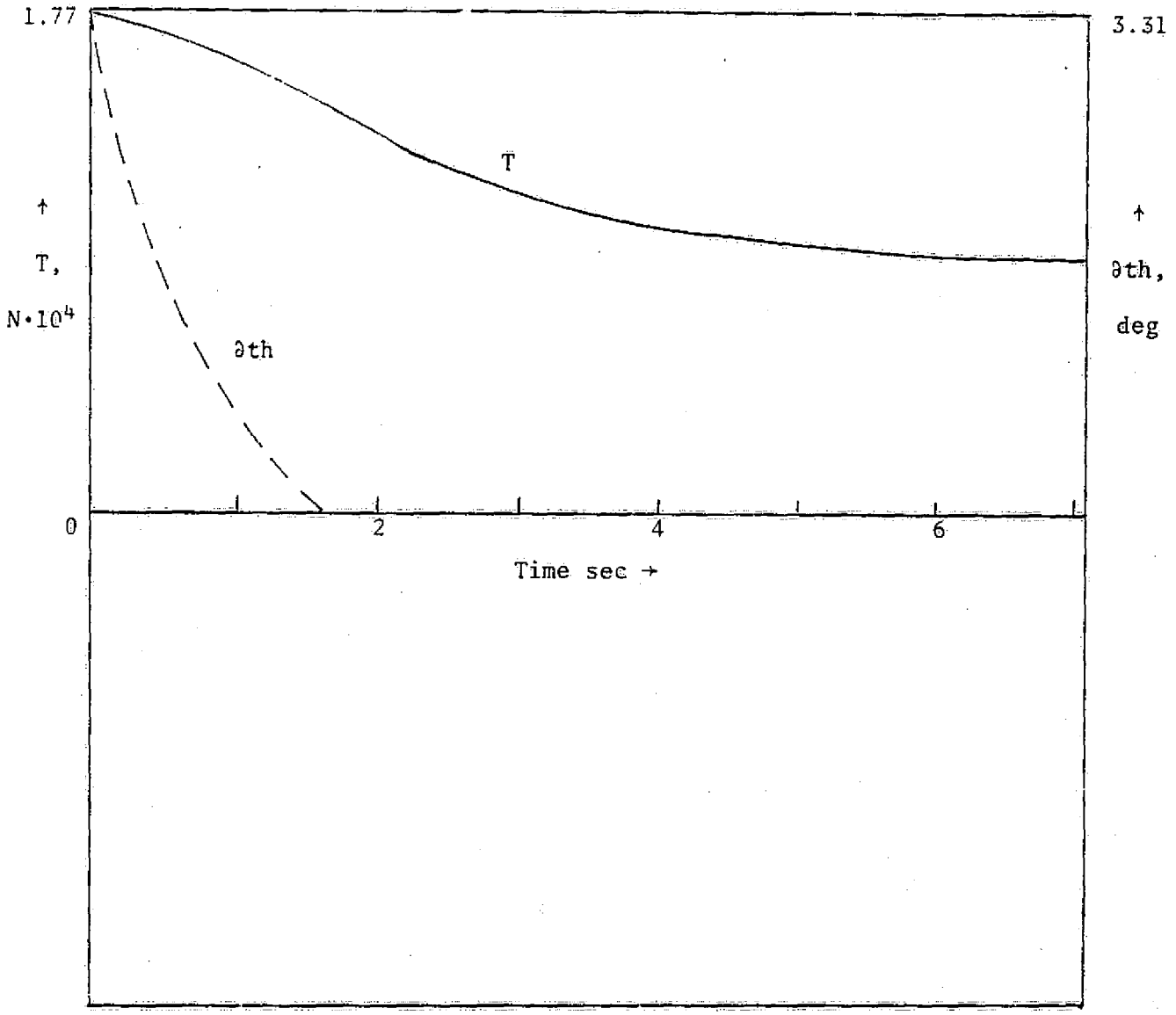

Figure 3(c). Flare response, -6° glide slope: thrust and throttle; no wind case, controller 1.

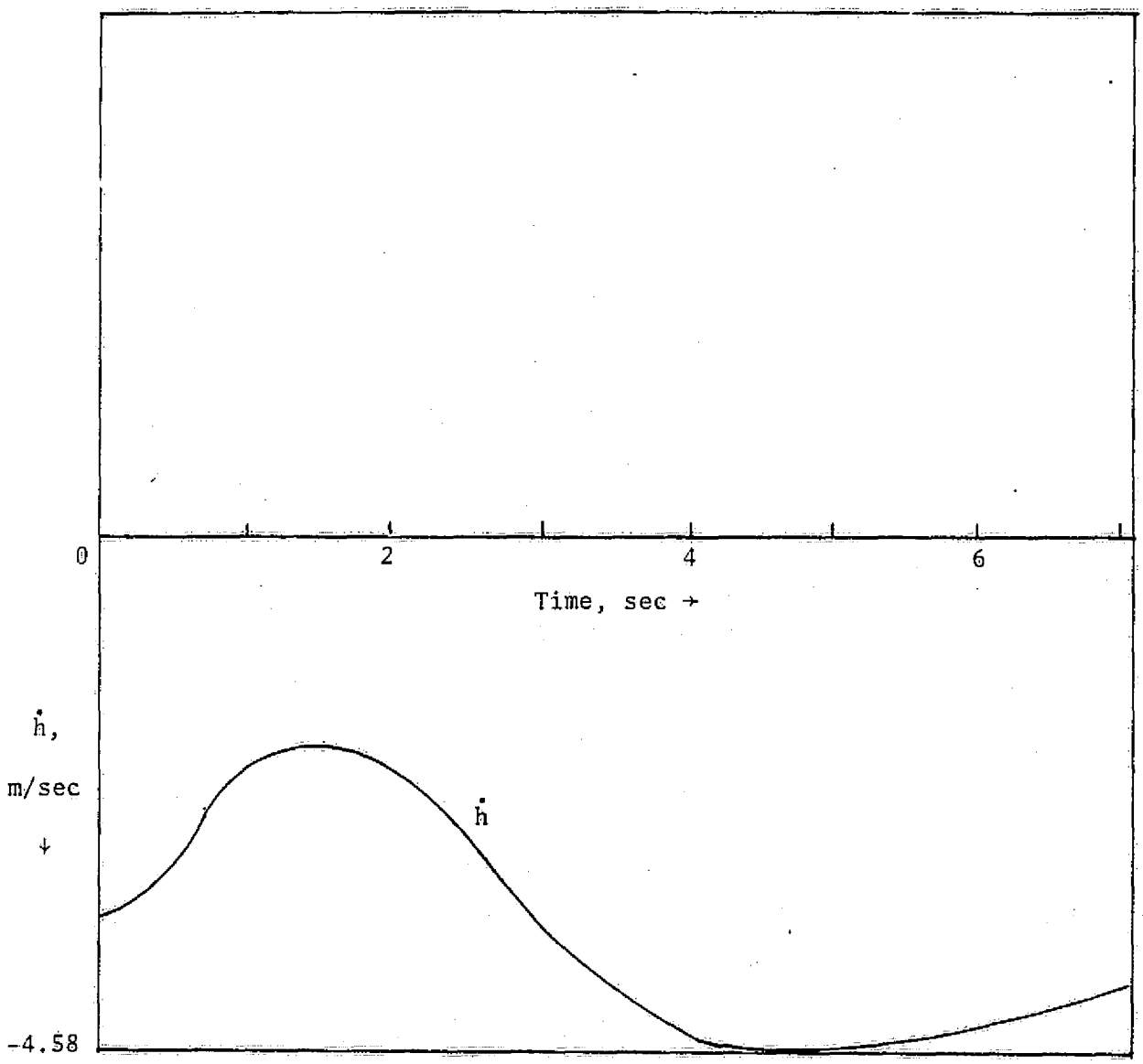

Figure 4(a). Glide slope capture, -3° glide slope: sink rate; wind profile A, controller 2A.

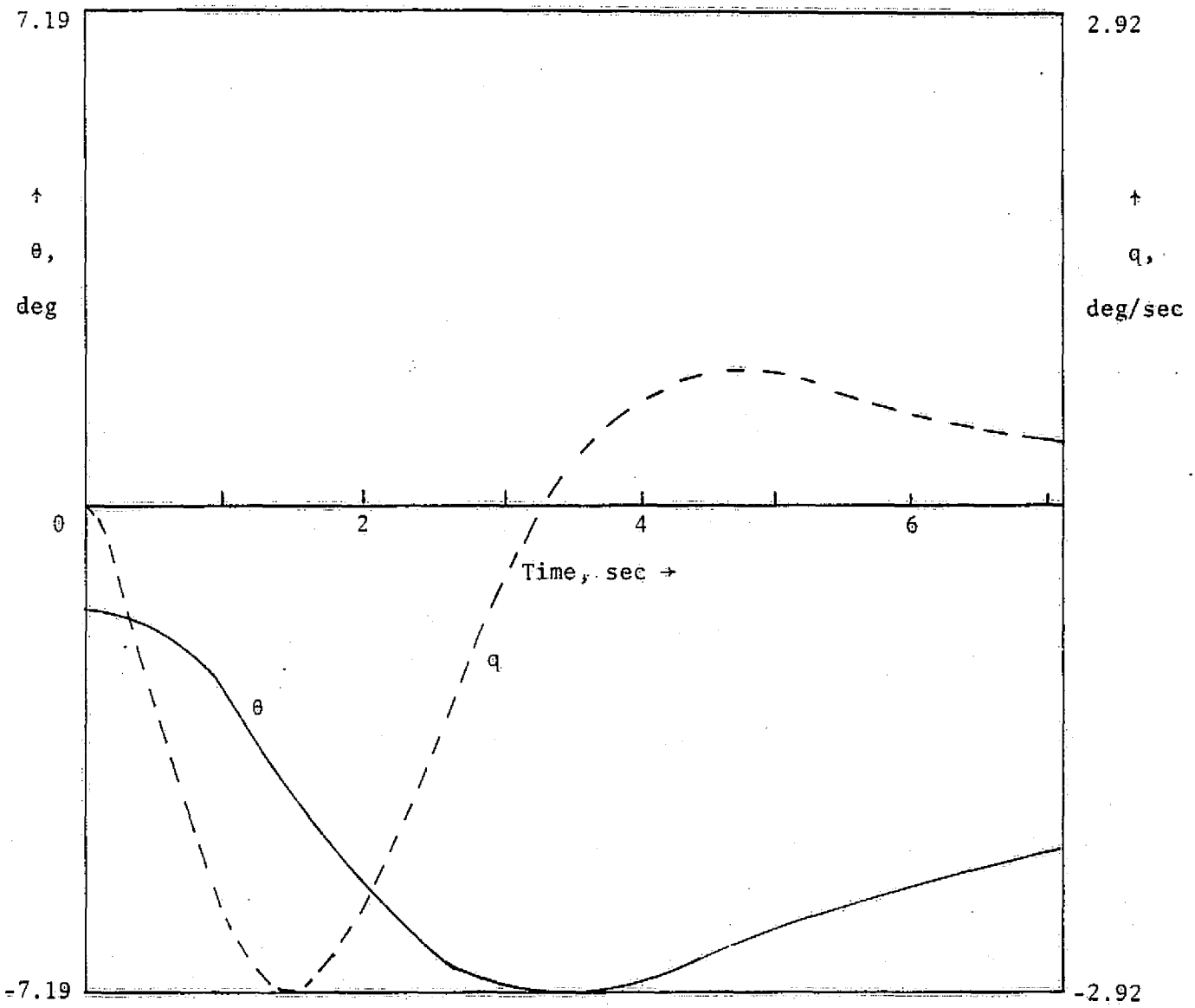

Figure 4(b). Glide slope capture, -3° glide slope: pitch and pitch rate; wind profile A, controller 2A.

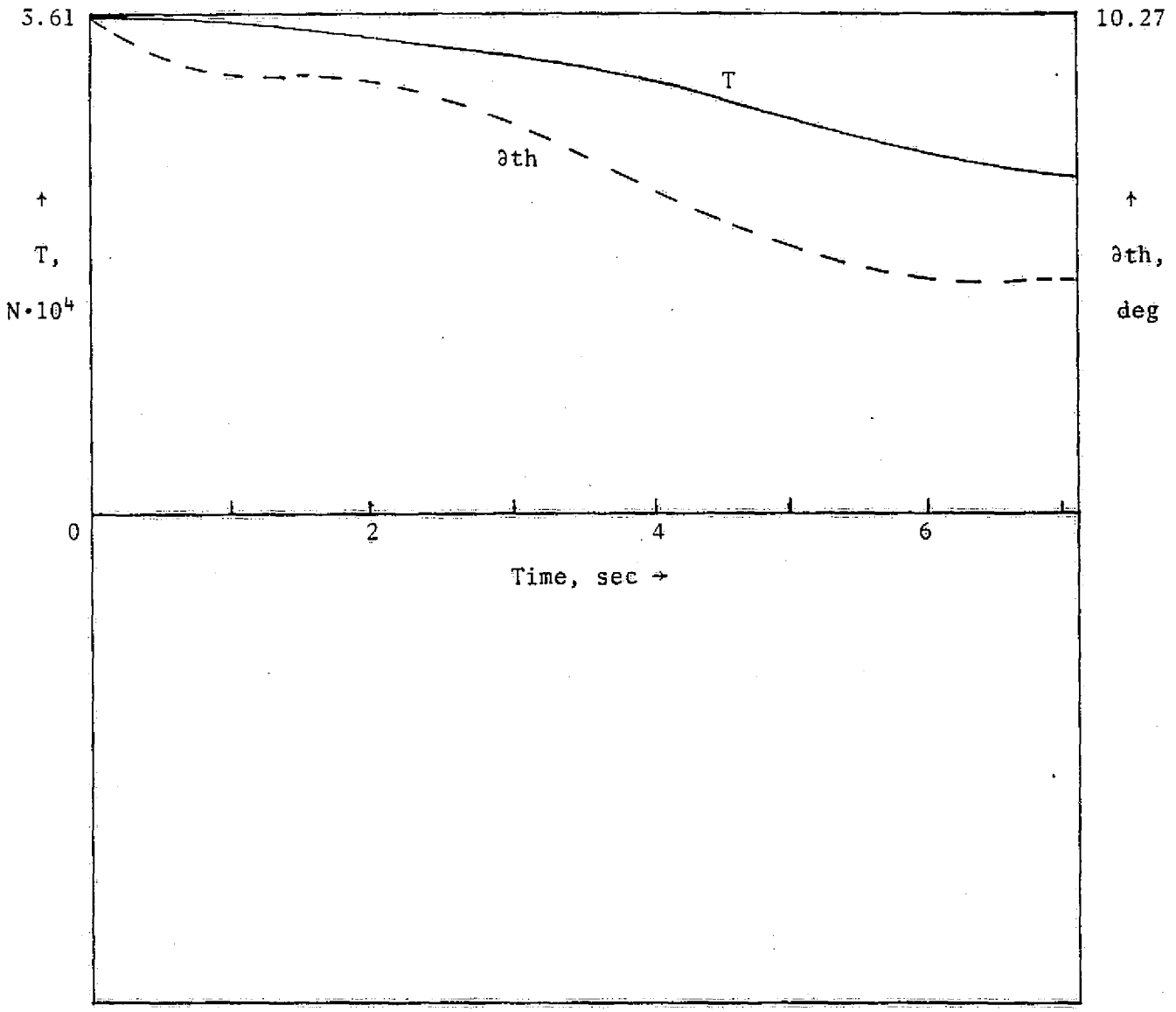

Figure 4(c). Glide slope capture, -3° glide slope: thrust and throttle; wind profile A, controller 2A

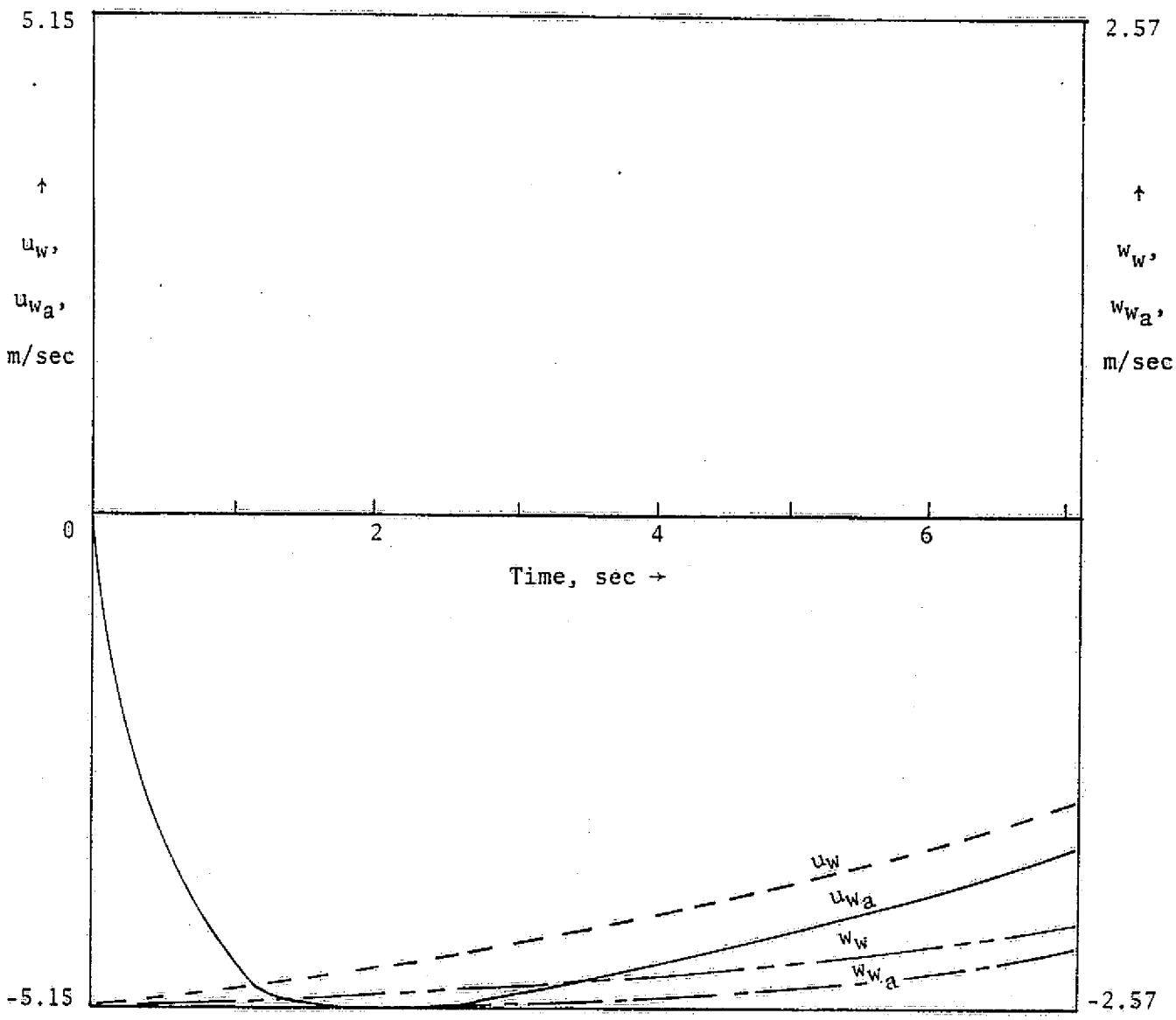

Figure 4(d). Glide slope capture, -3° glide slope: wind velocities at the wing; wind profile A, controller 2A.

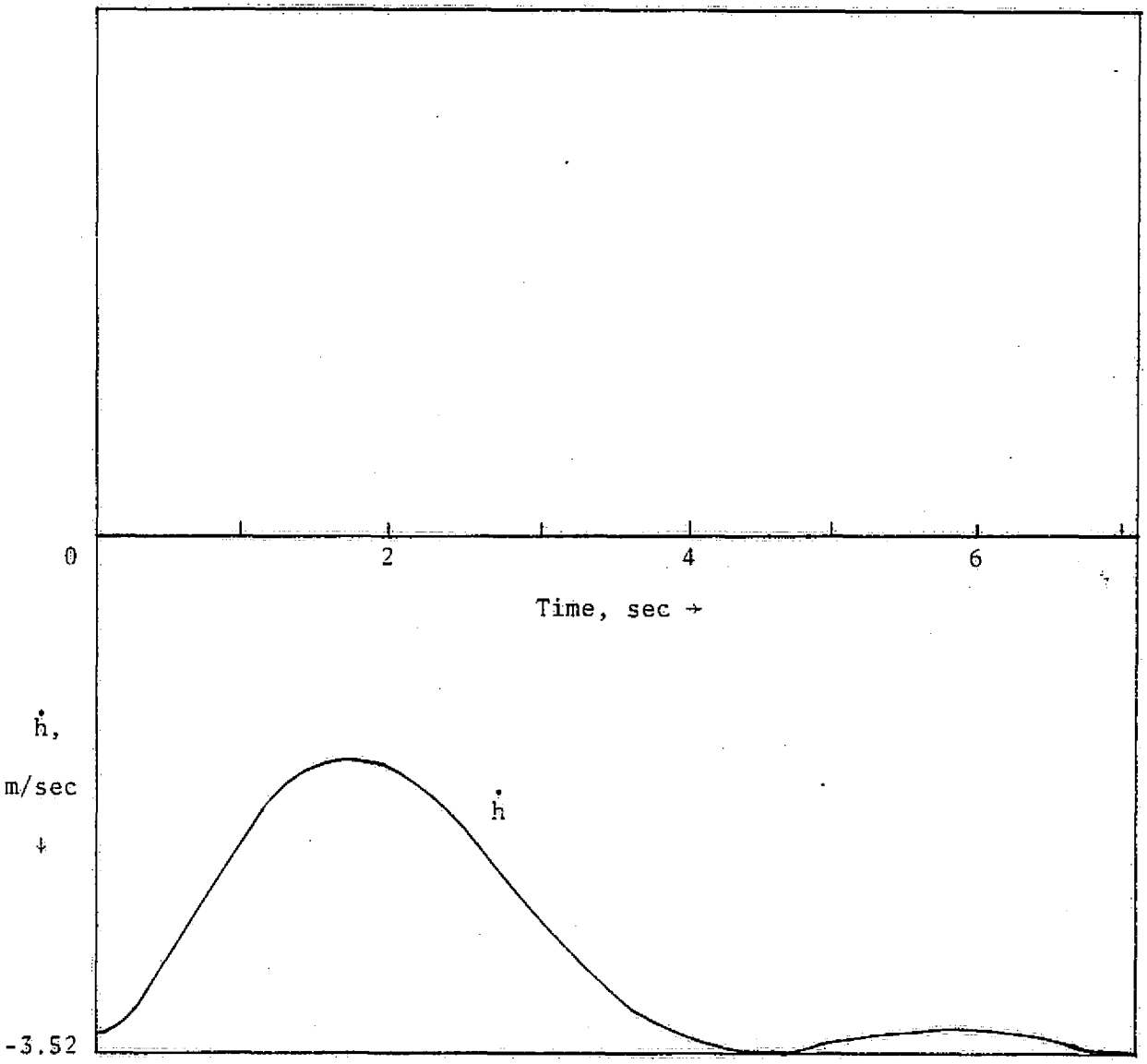

Figure 5(a). Glide slope capture, -3° glide slope: sink rate; wind profile A, controller 2B.

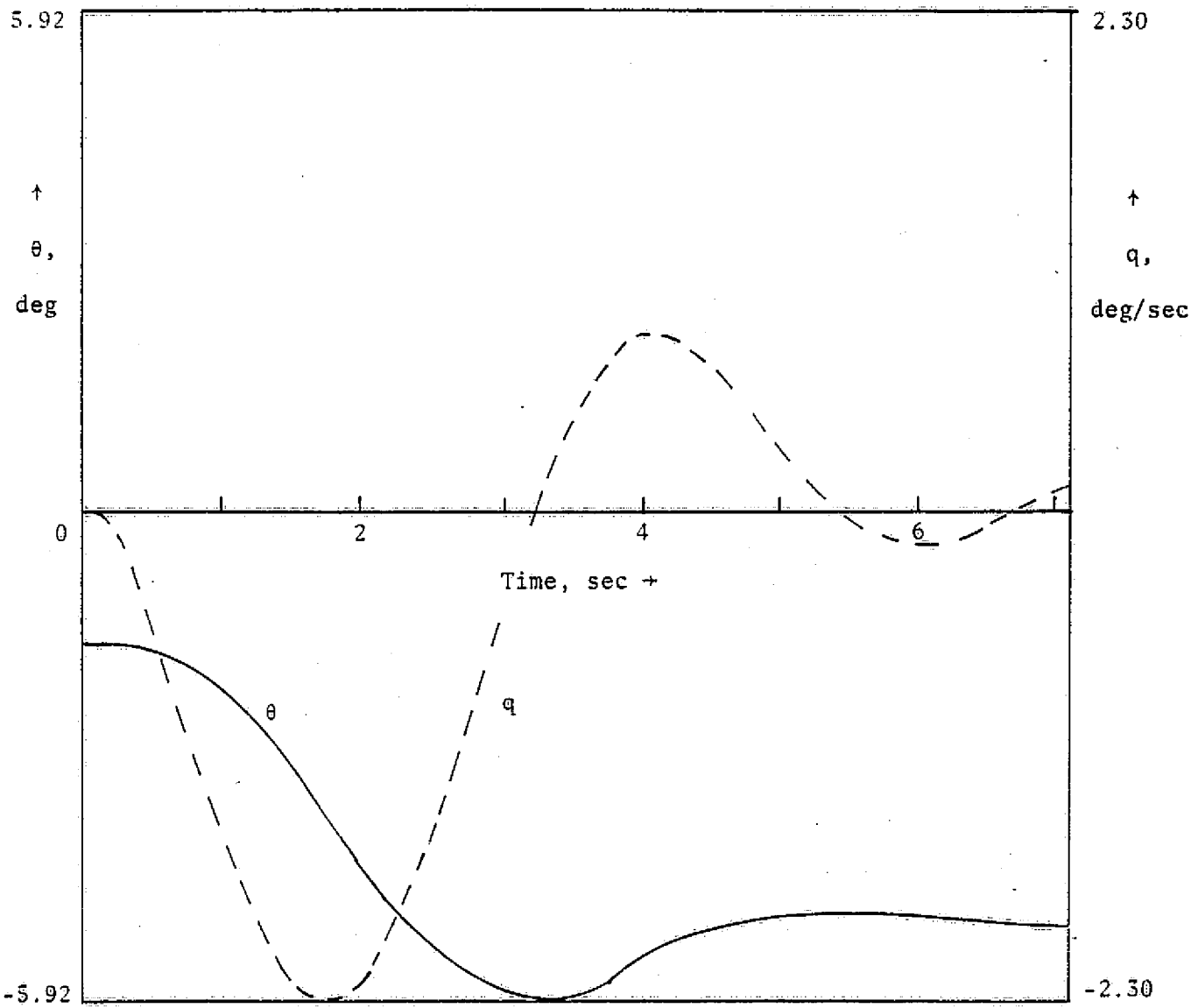

Figure 5(b). Glide slope capture, -3° glide slope: pitch and pitch rate; wind profile A, controller 2B.

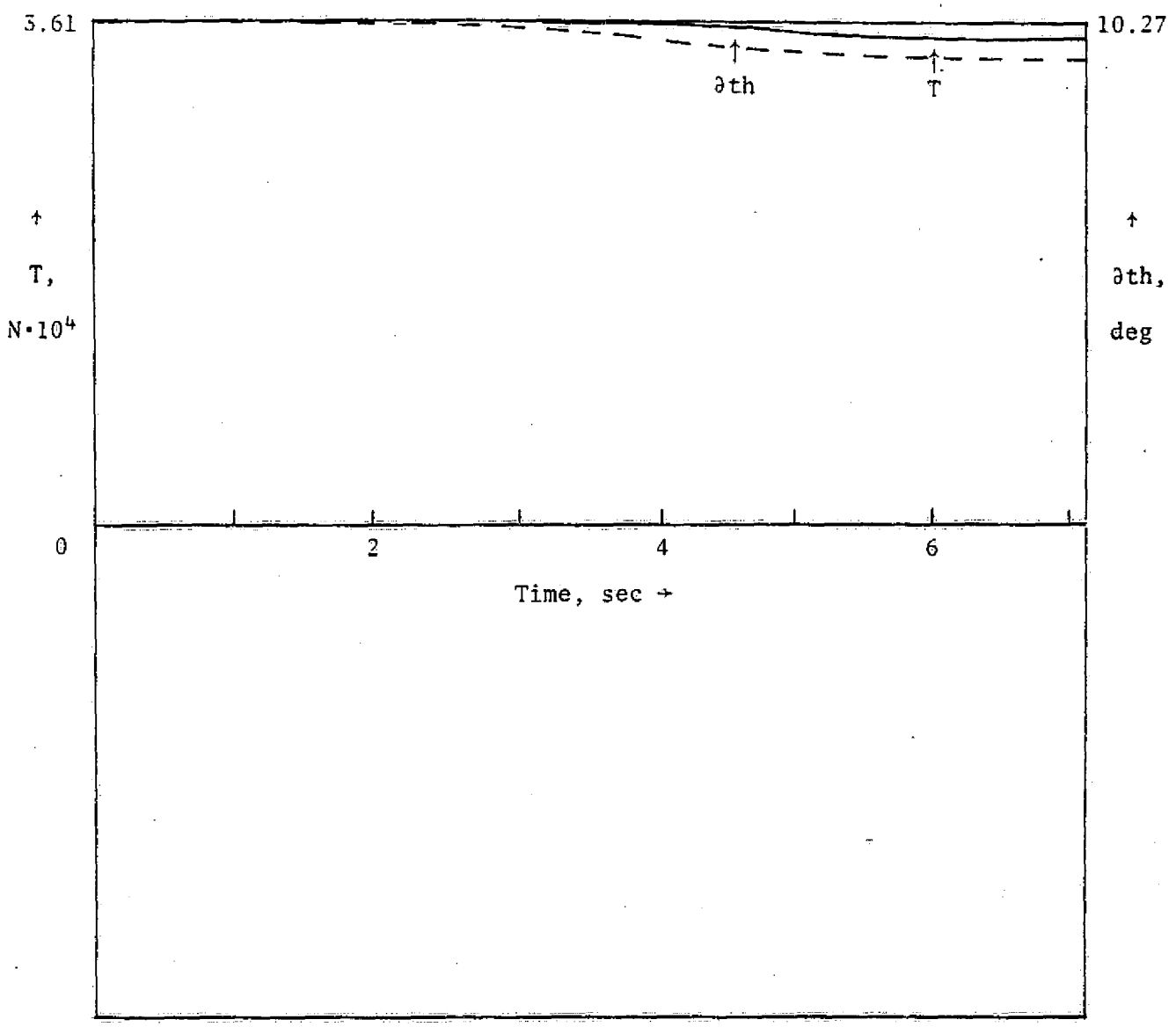

Figure 5(c). Glide slope capture, -3° glide slope: thrust and throttle; wind profile A, controller 2B.

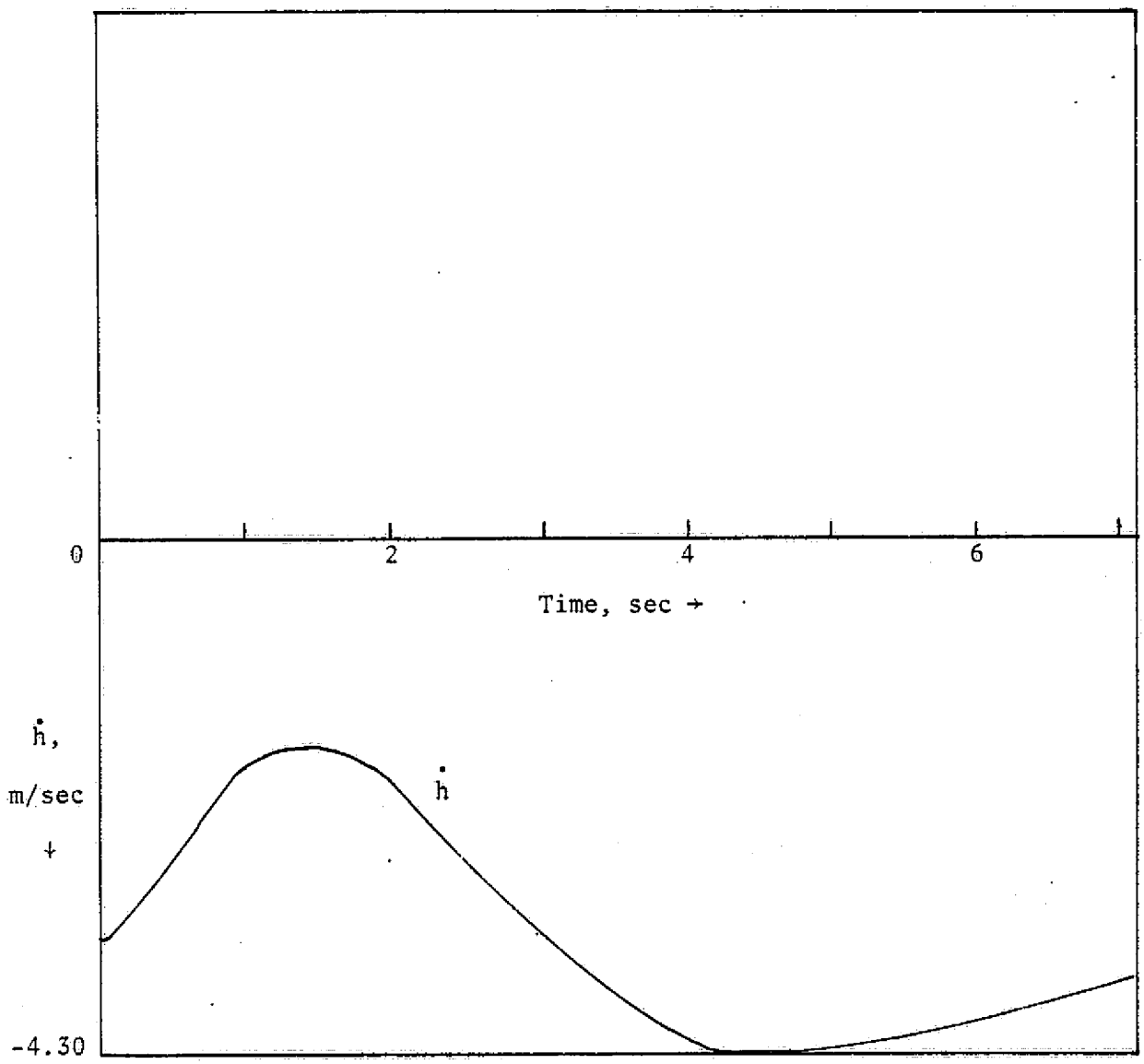

Figure 6(a). Glide slope capture, -3° glide slope: sink rate; wind profile A, controller 2F.

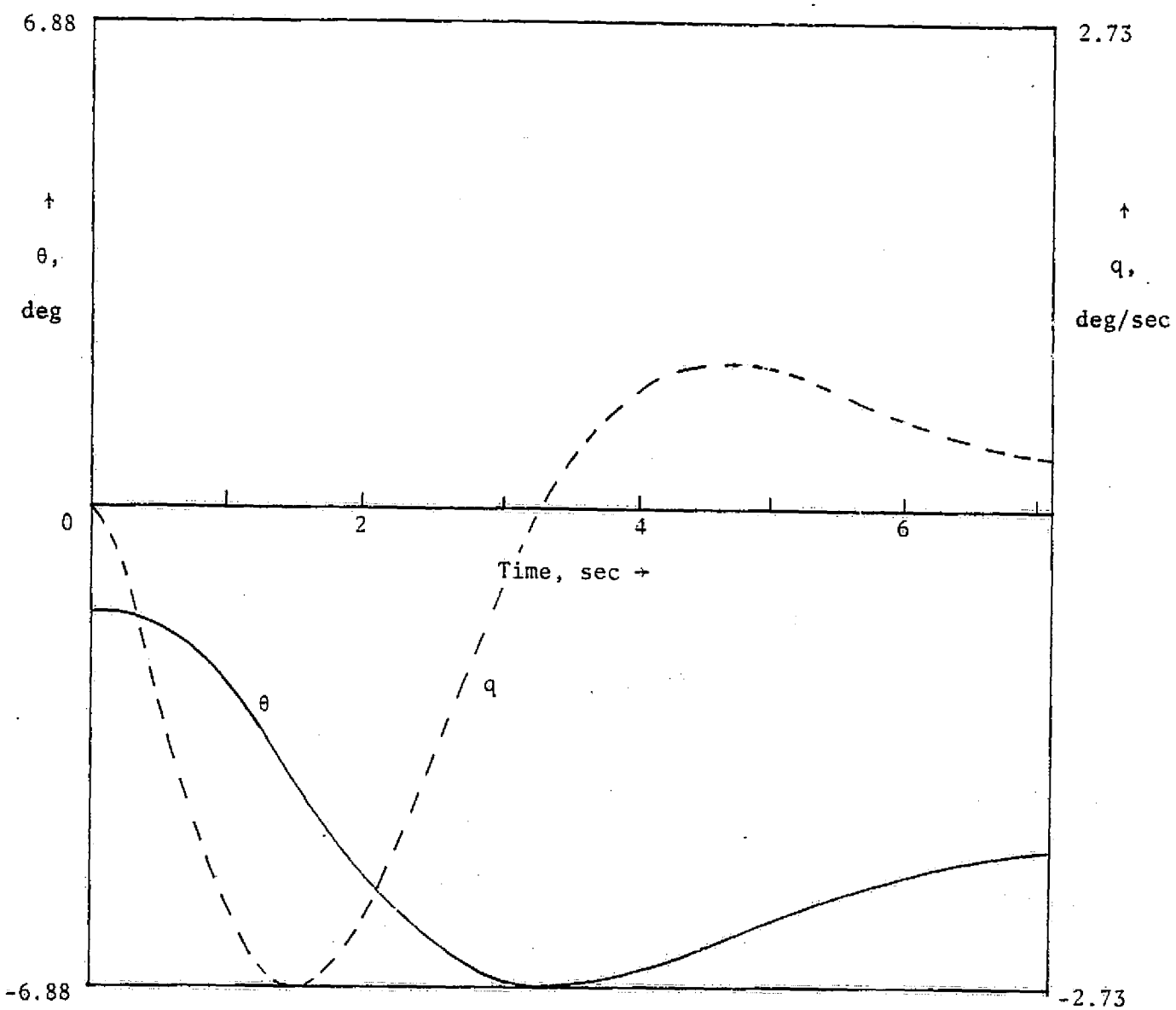

Figure 6(b). Glide slope capture, -3° glide slope: pitch and pitch rate; wind profile A, controller 2F.

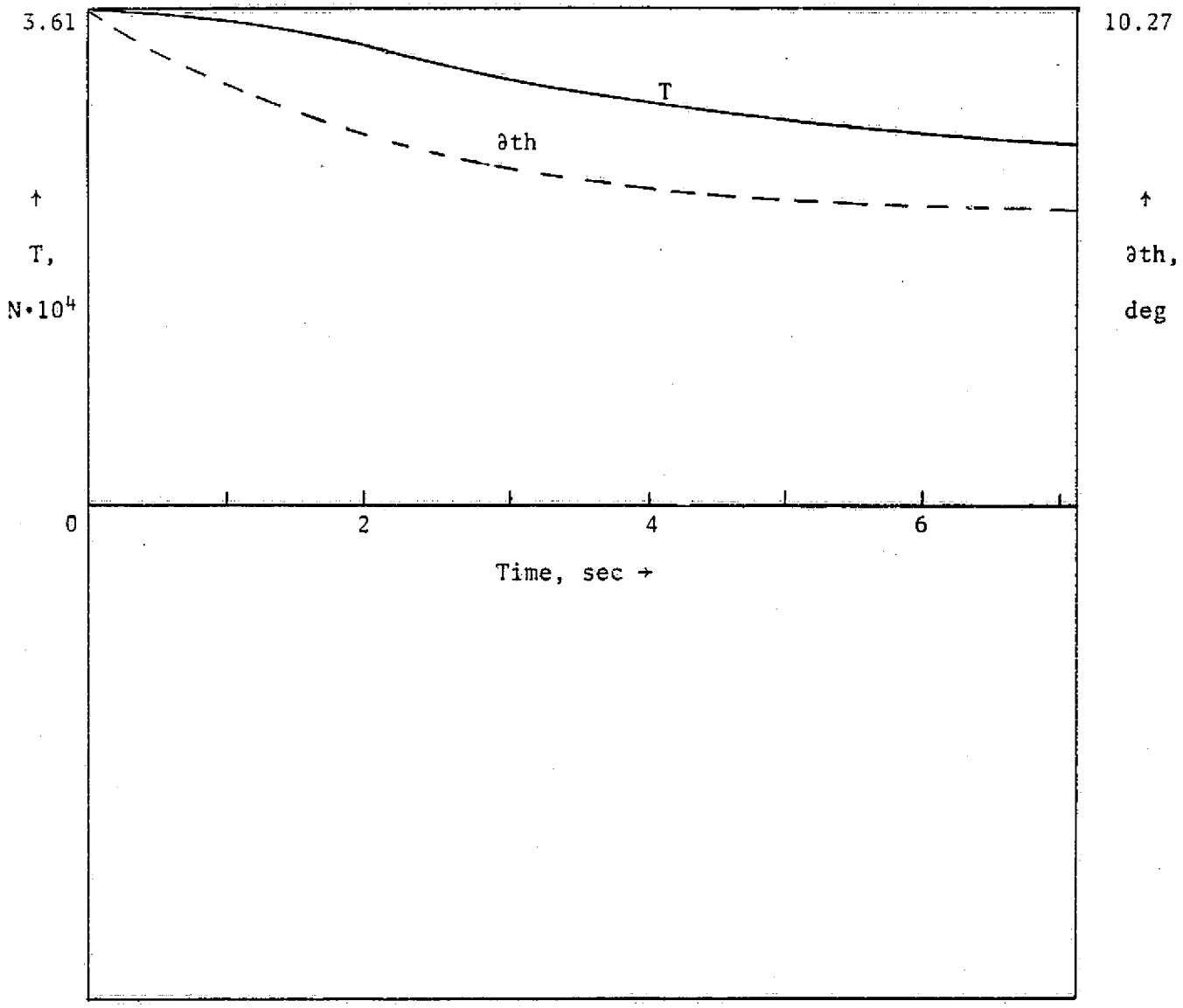

Figure 6(c). Glide slope capture, -3° glide slope: thrust and throttle; wind profile A, controller 2F.

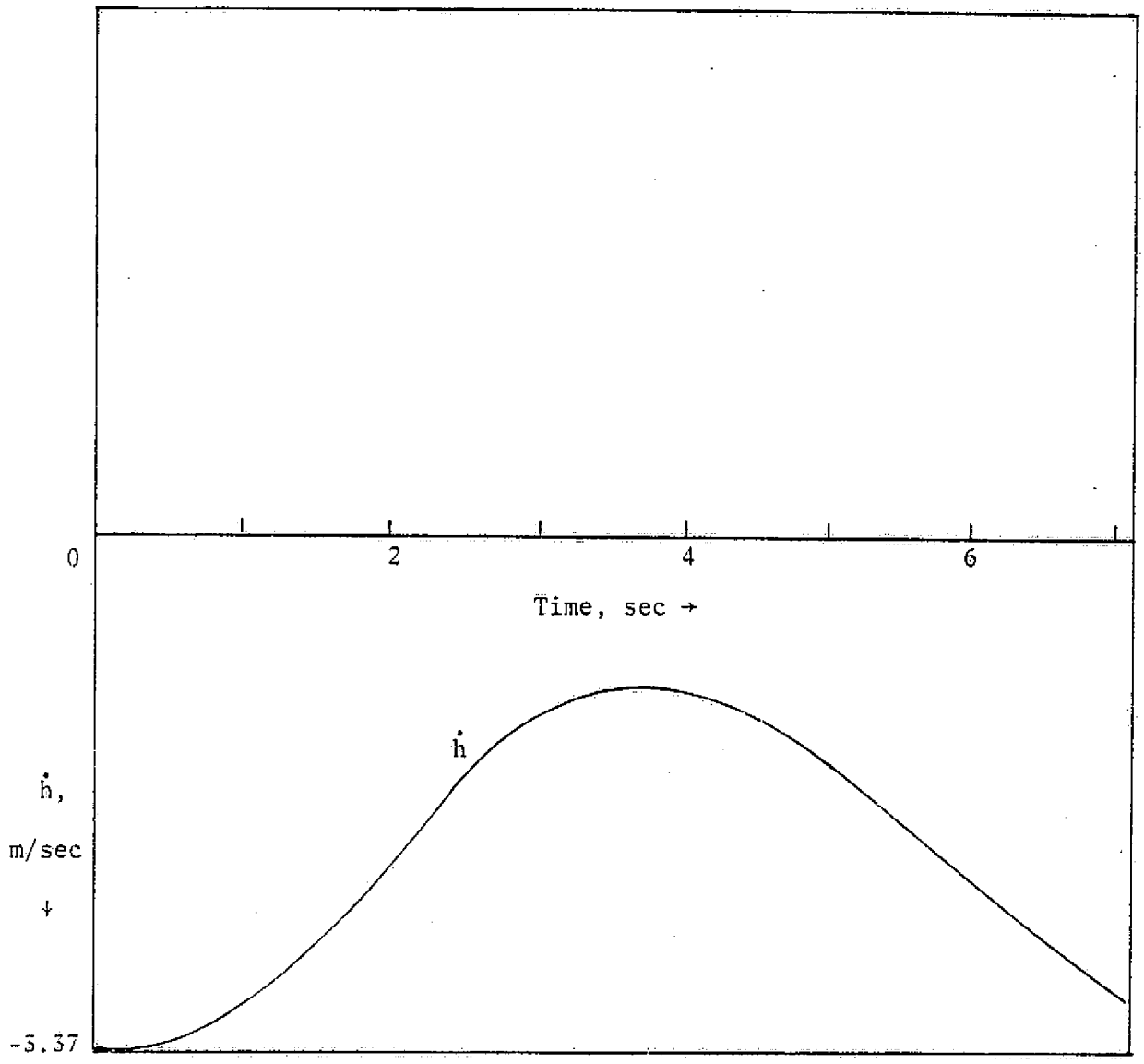

Figure 7(a). Glide slope capture, -3° glide slope: sink rate; wind profile B, controller 2A.

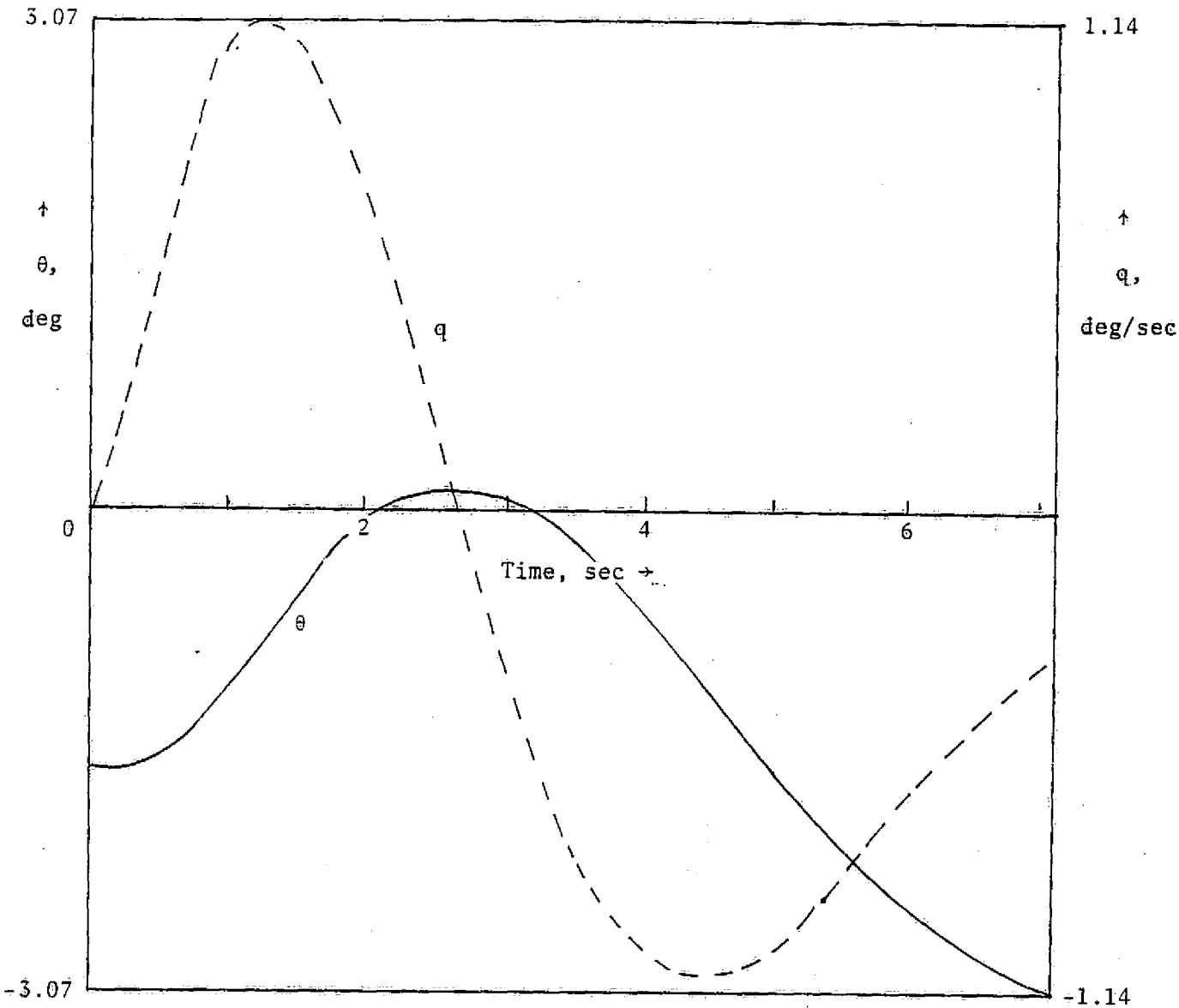

Figure 7(b). Glide slope capture, -3° glide slope: pitch and pitch rate; wind profile B, controller 2A.

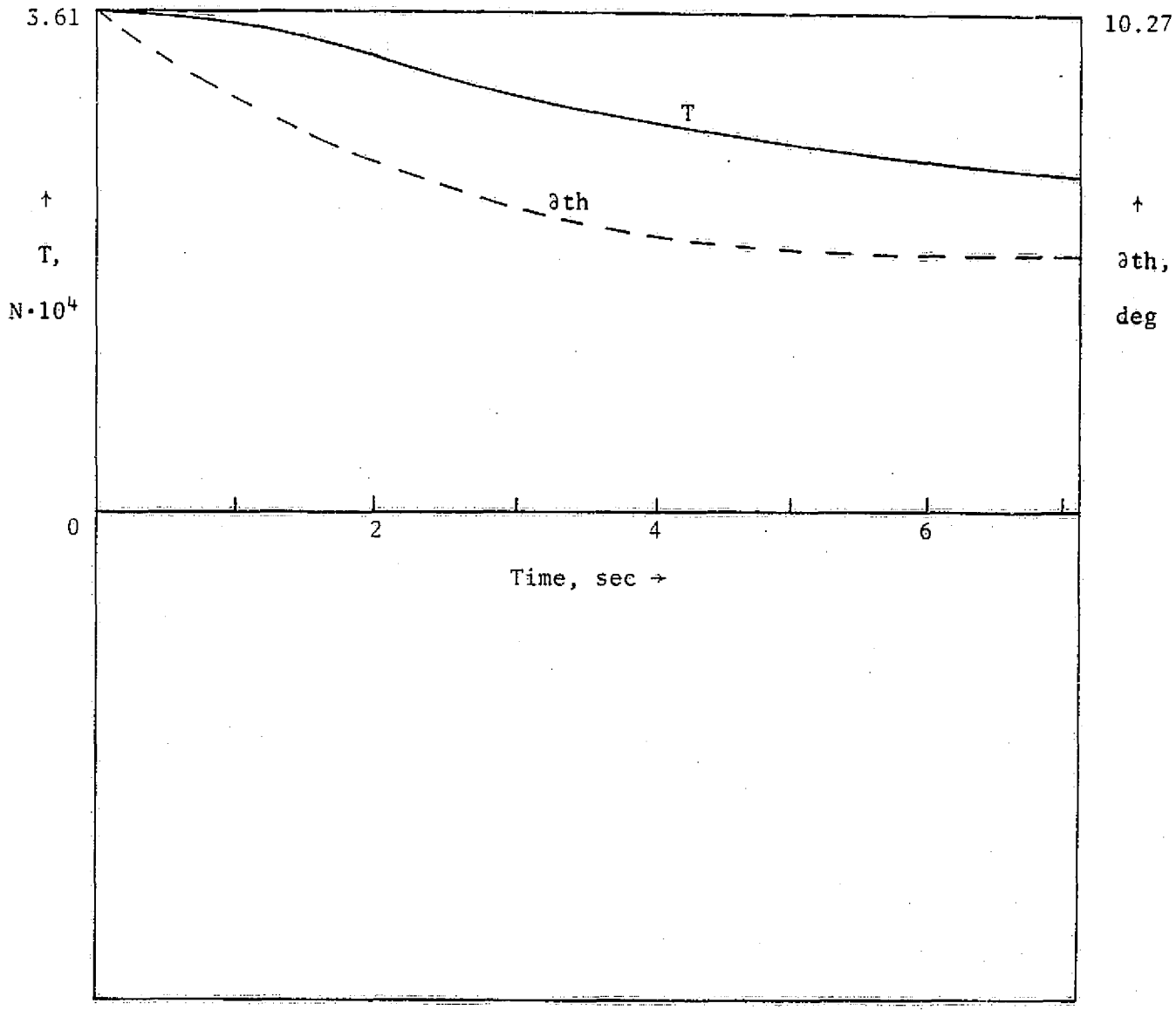

Figure 7(c). Glide slope capture, -3° glide slope: thrust and throttle; wind profile B, controller 2A.

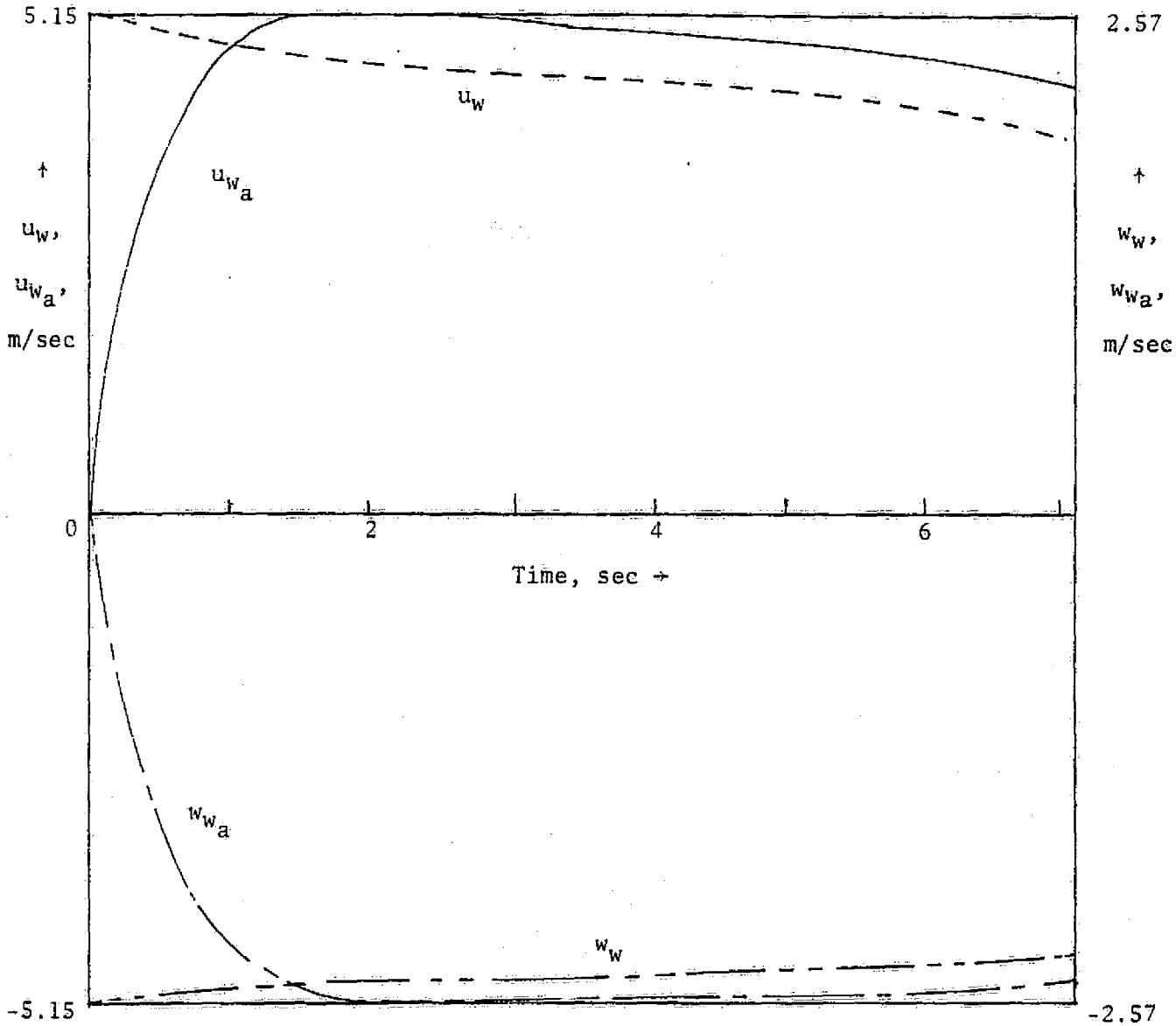

Figure 7(d). Glide slope capture, -3° glide slope: wind velocities at the wing; wind profile B, controller 2A.

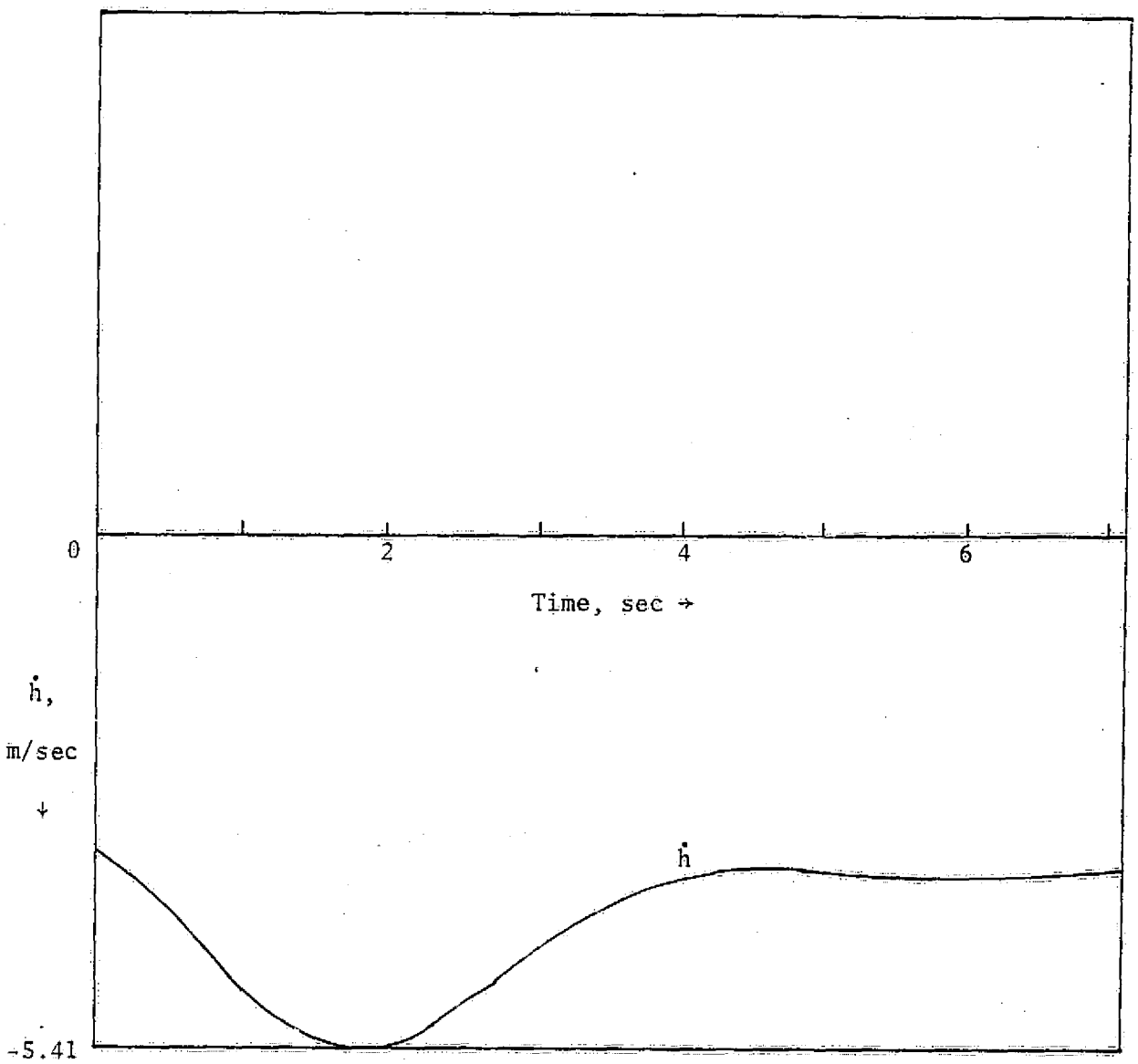

Figure 8(a). Glide slope capture, -3° glide slope: sink rate; wind profile C, controller 2B.

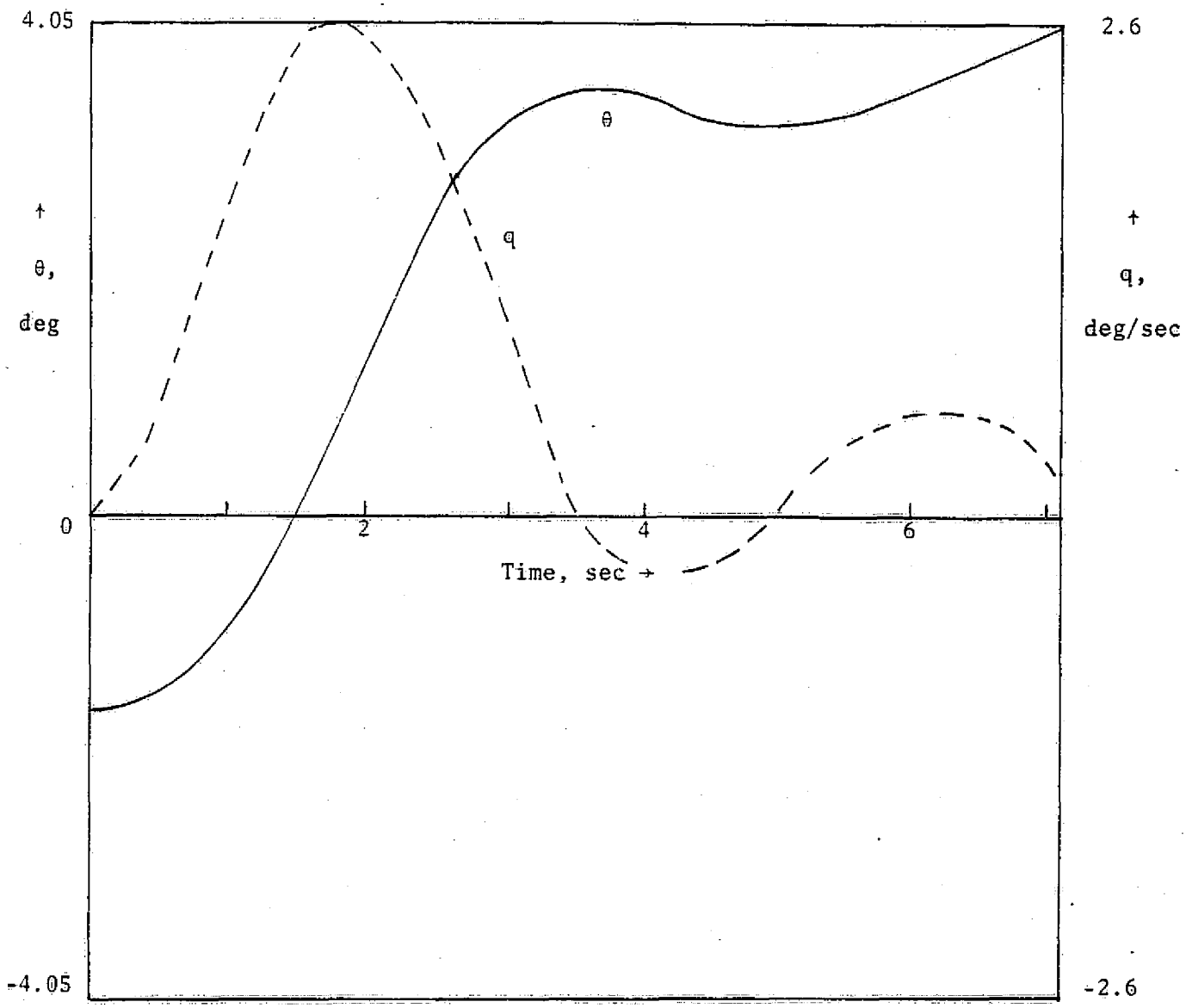

Figure 8(b). Glide slope capture, -3° glide slope: pitch and pitch rate; wind profile C, controller 2B.

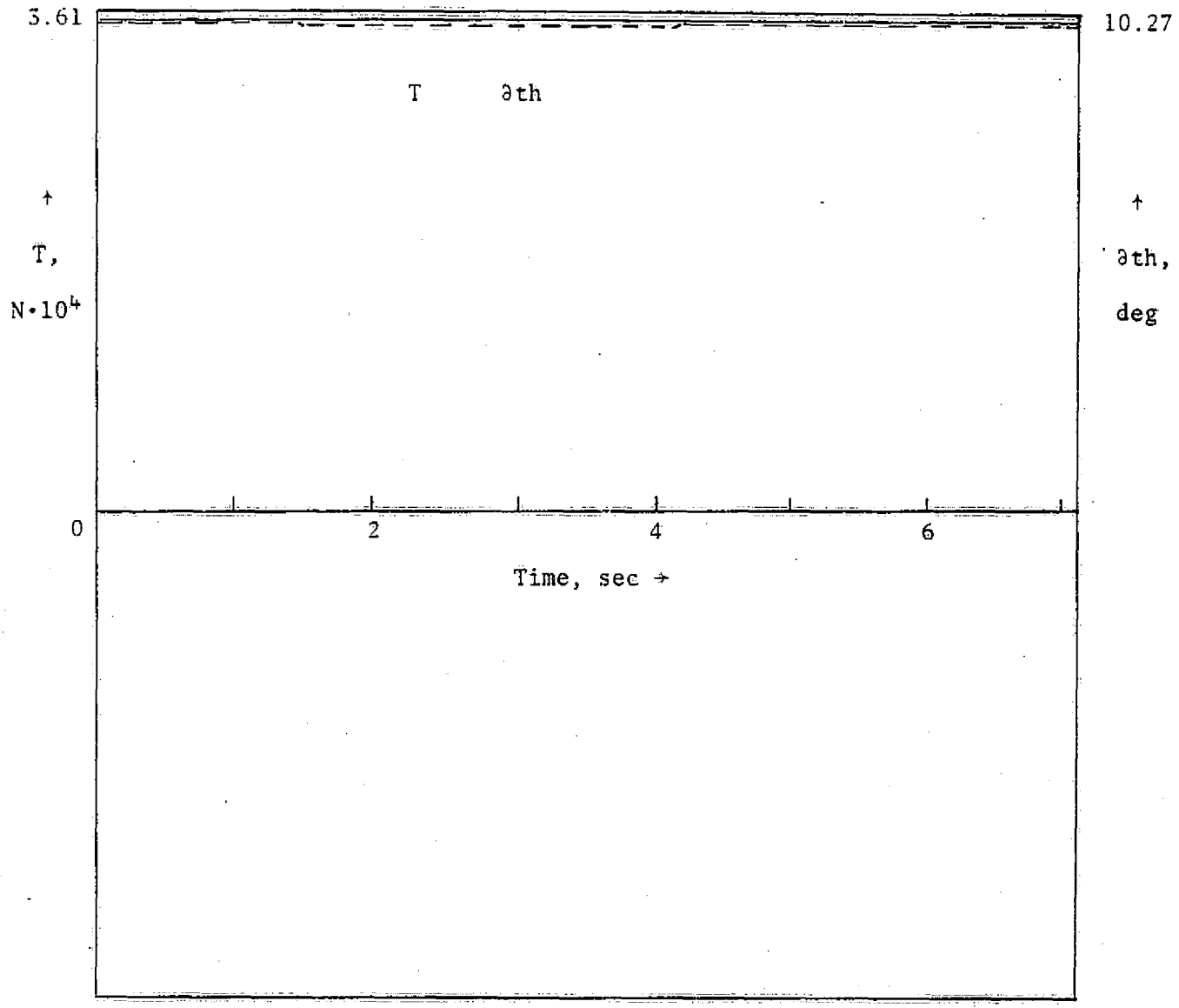

Figure 8(c). Glide slope capture, -3° glide slope: thrust and throttle; wind profile C, controller 2B.

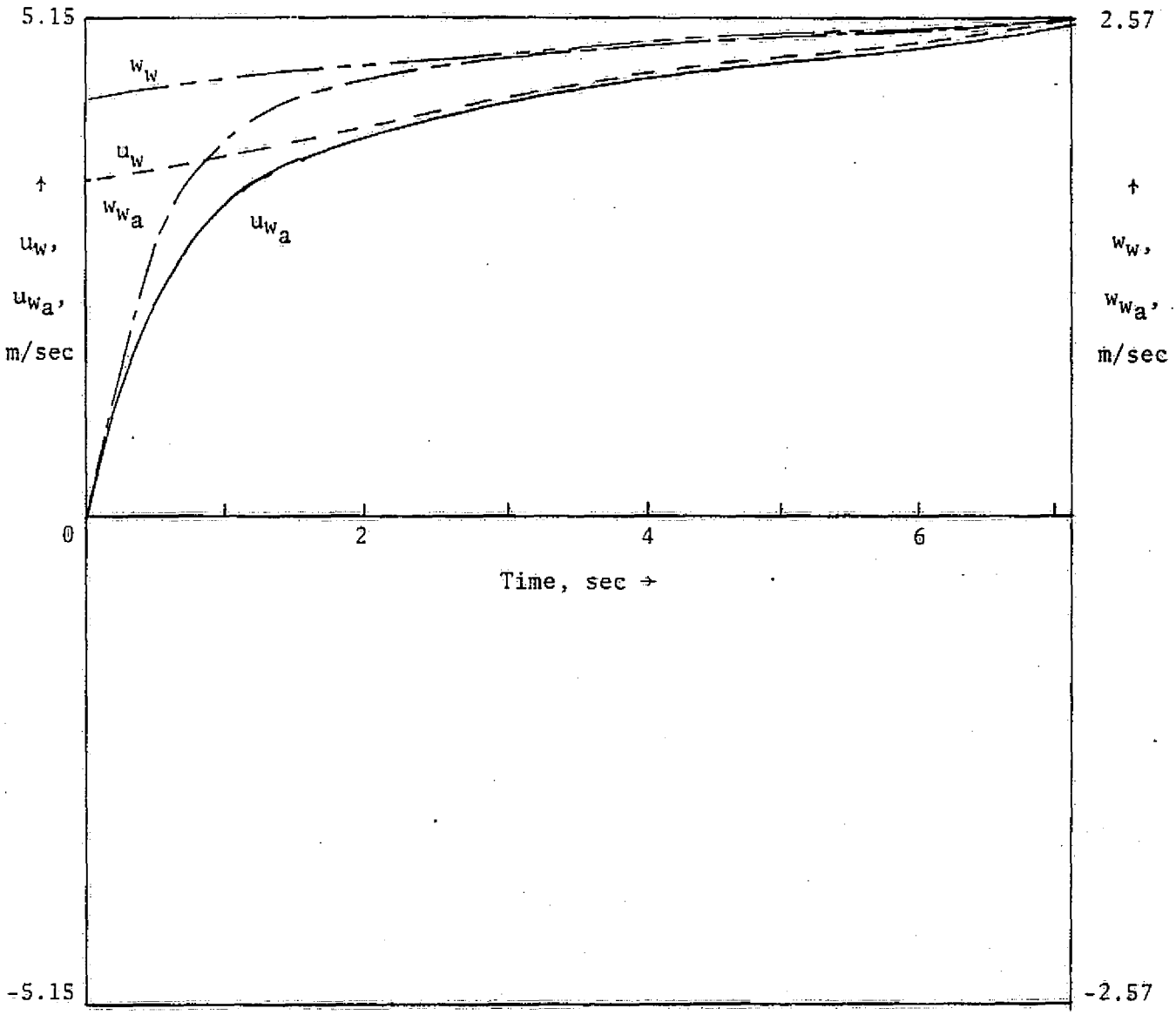

Figure 8(d). Glide slope capture, -3° glide slope: wind velocities at the wing; wind profile C, controller 2B.

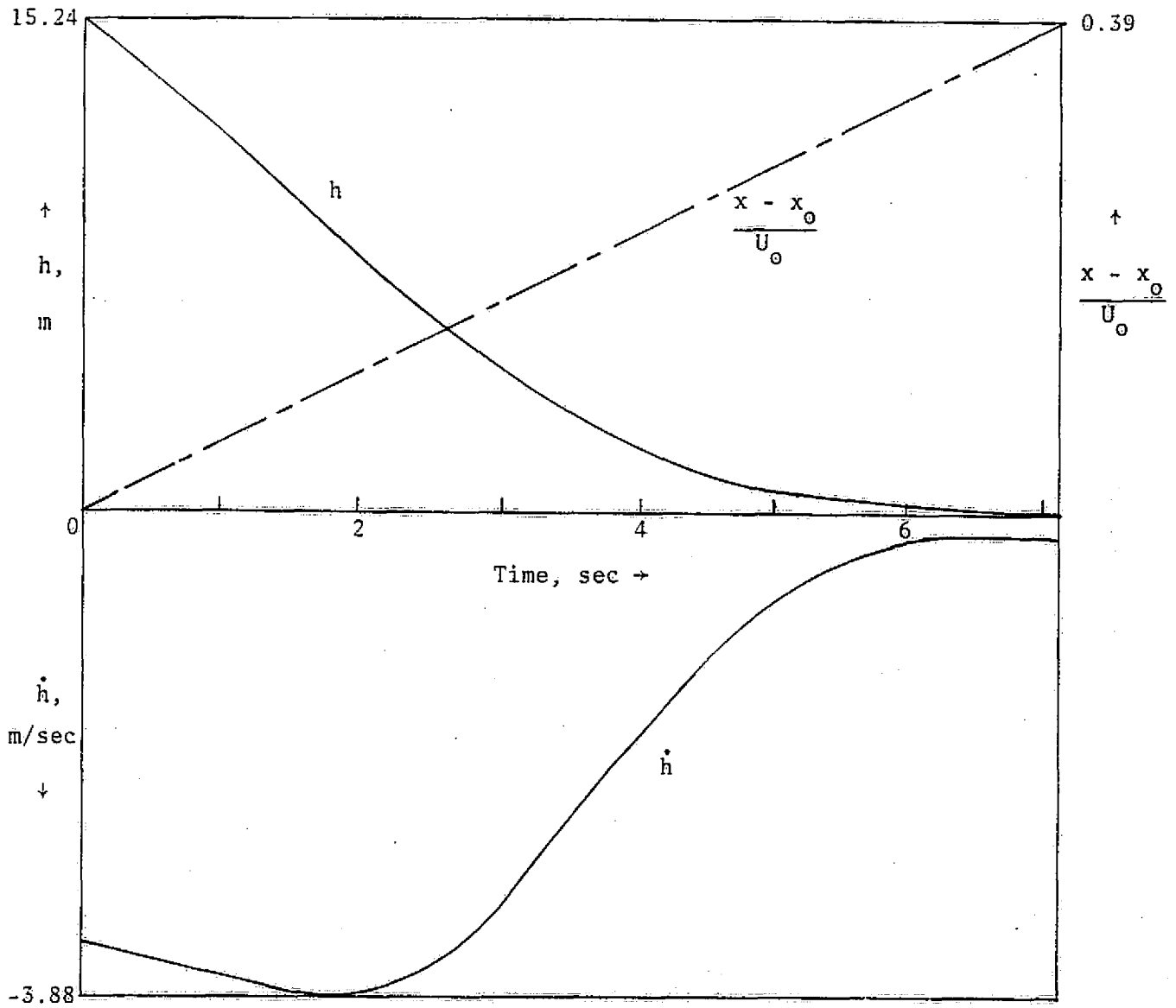

Figure 9(a). Flare response, -3° glide slope: altitude, sink rate, and horizontal dispersion; wind profile A, controller 2F.

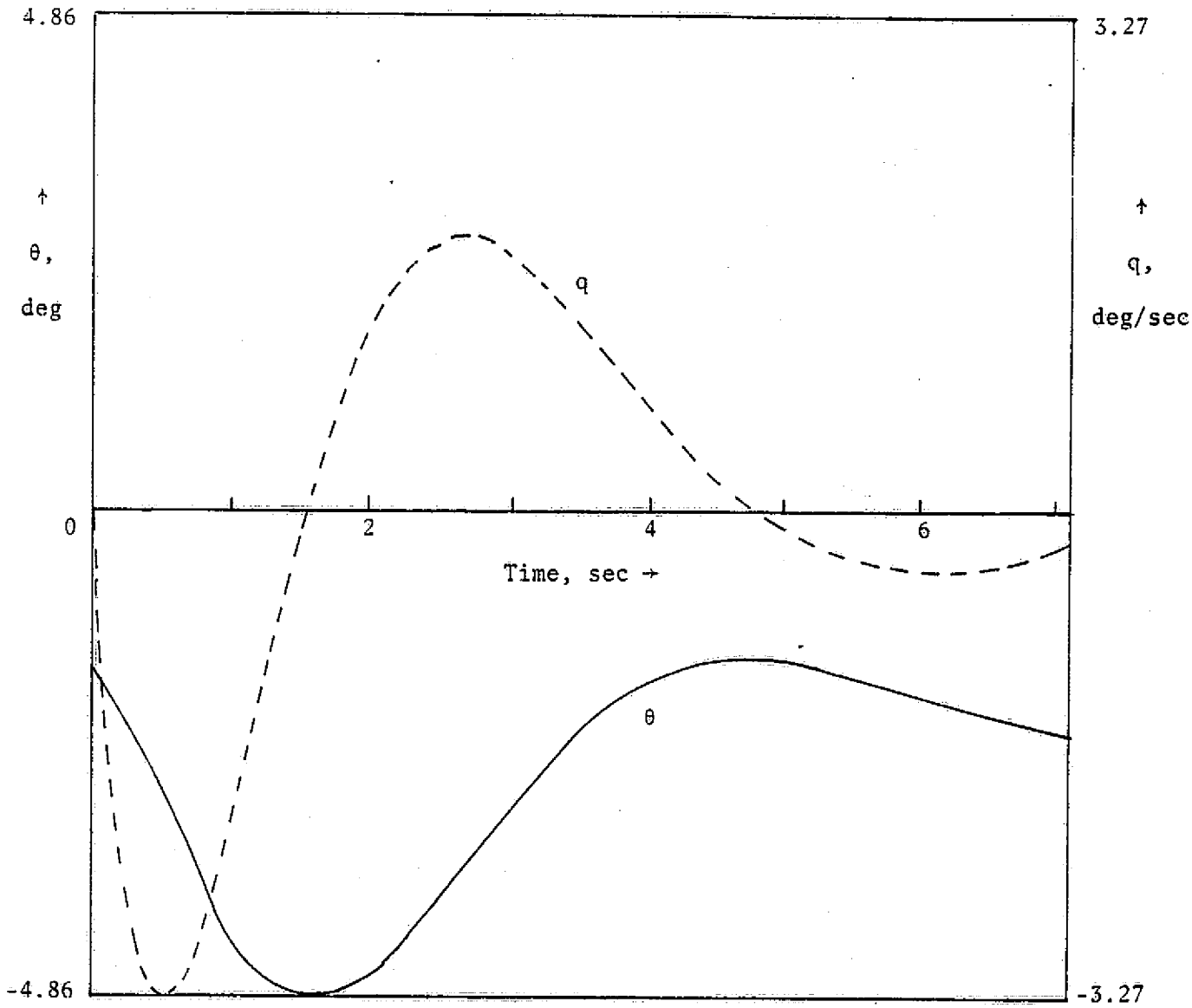

Figure 9(b). Flare response, -3° glide slope: pitch and pitch rate; wind profile A, controller 2F.

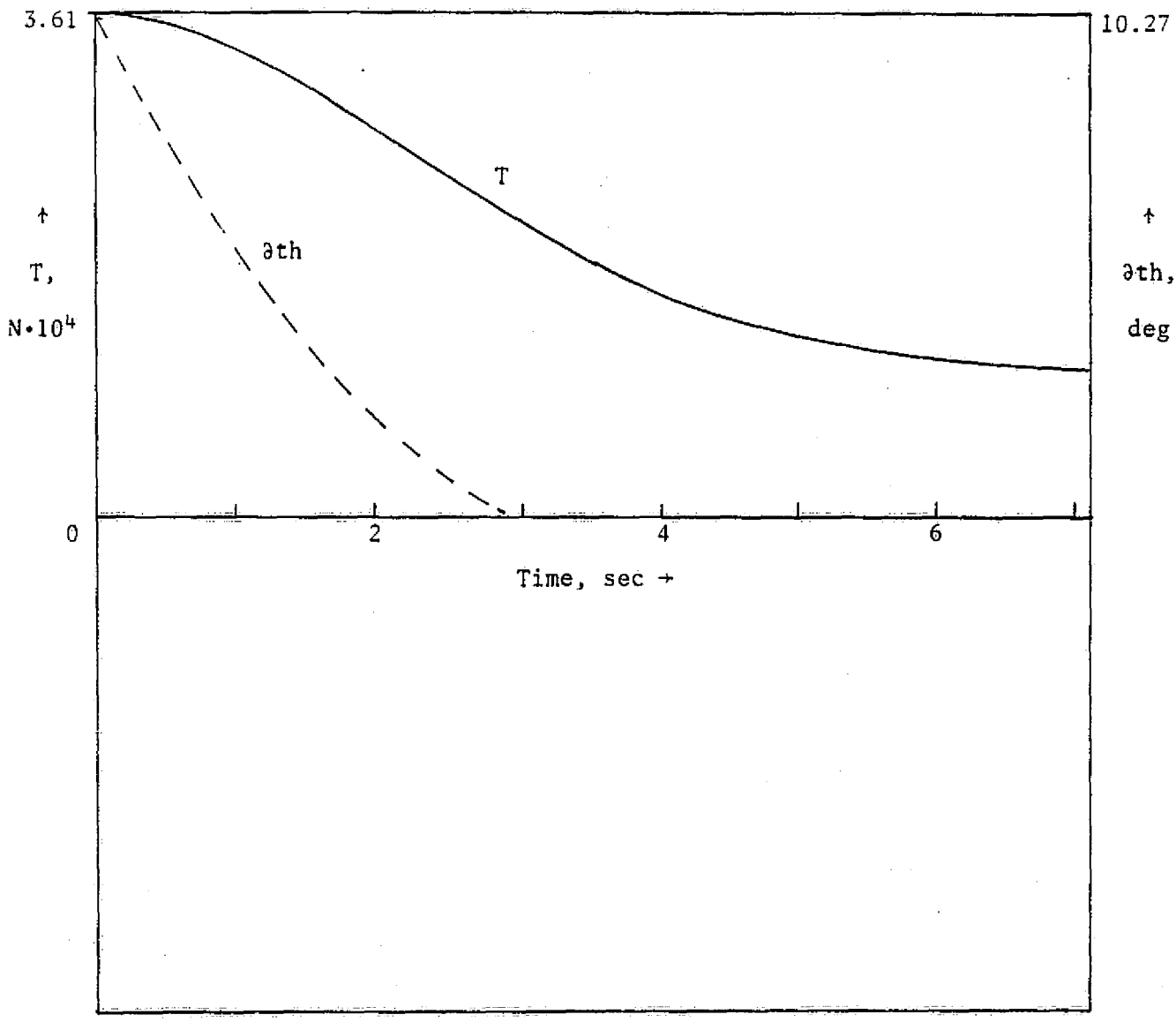

Figure 9(c). Flare response, -3° glide slope: thrust and throttle; wind profile A, controller 2F.

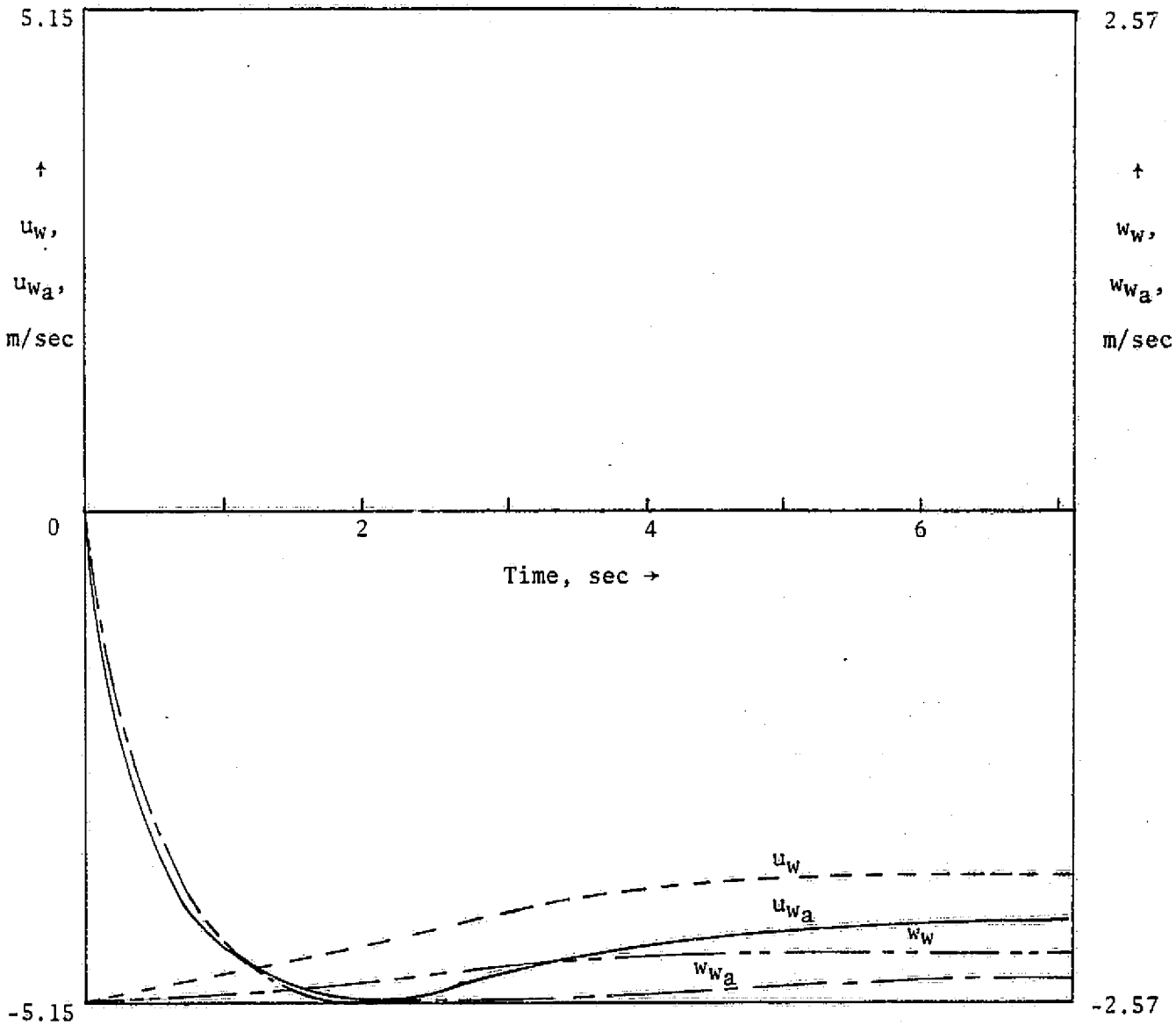

Figure 9(d). Flare response, -3° glide slope: wind velocities at the wing; wind profile A, controller 2F.

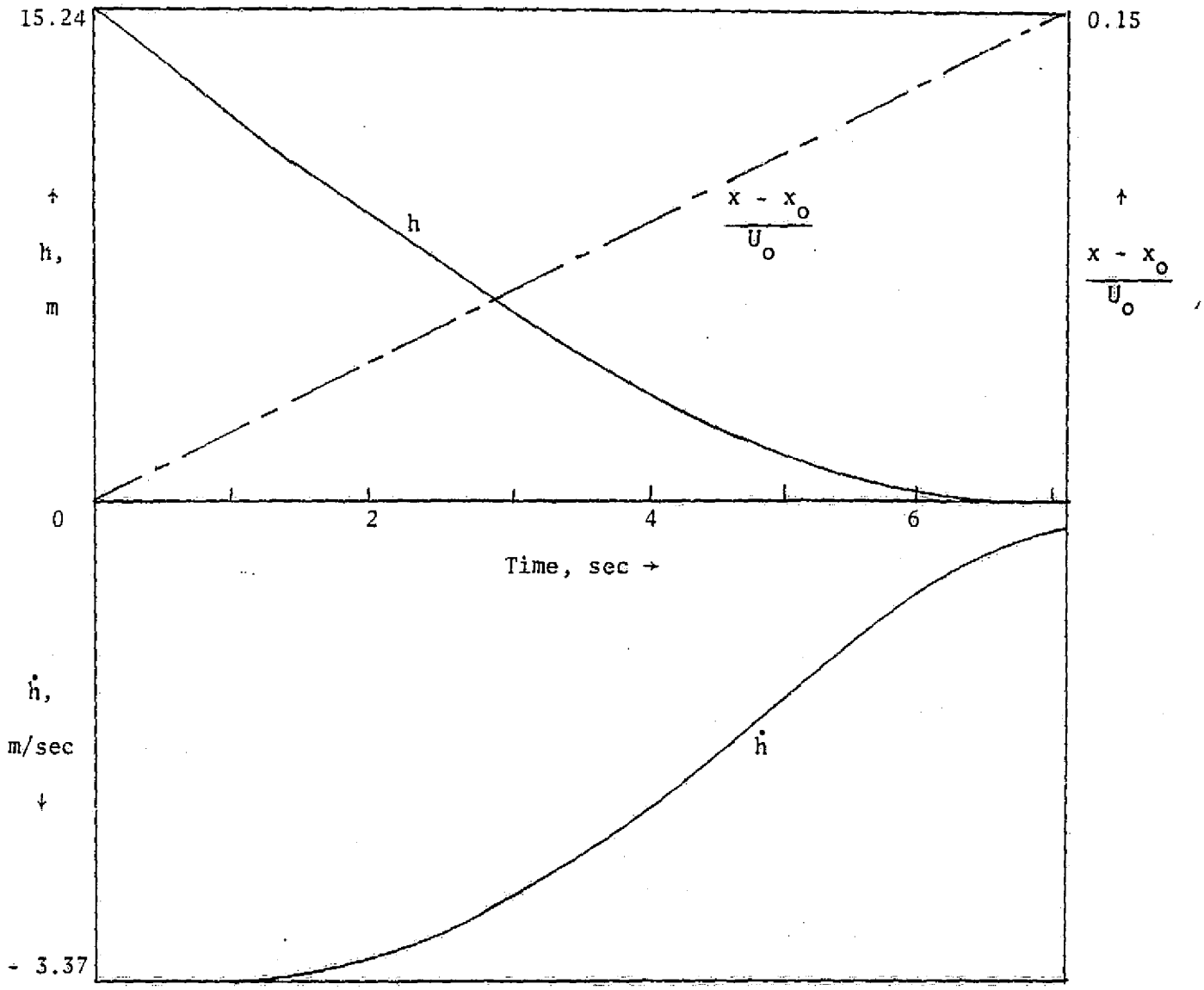

Figure 10(a). Flare response, -3° glide slope: altitude, sink rate, and horizontal dispersion; no wind case, controller 3.

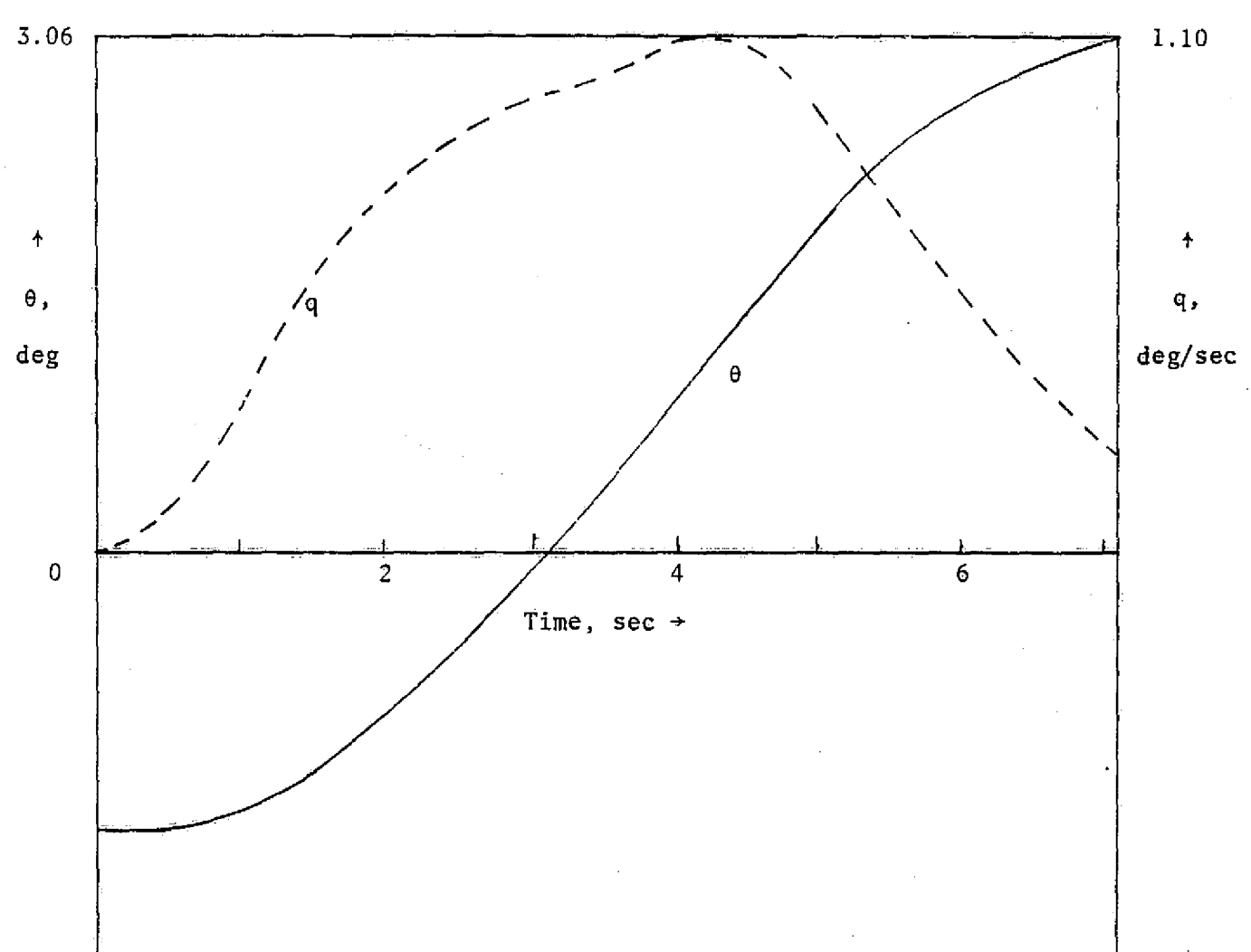

Figure 10(b). Flare response, -3° glide slope: pitch and pitch rate; no wind case, controller 3.

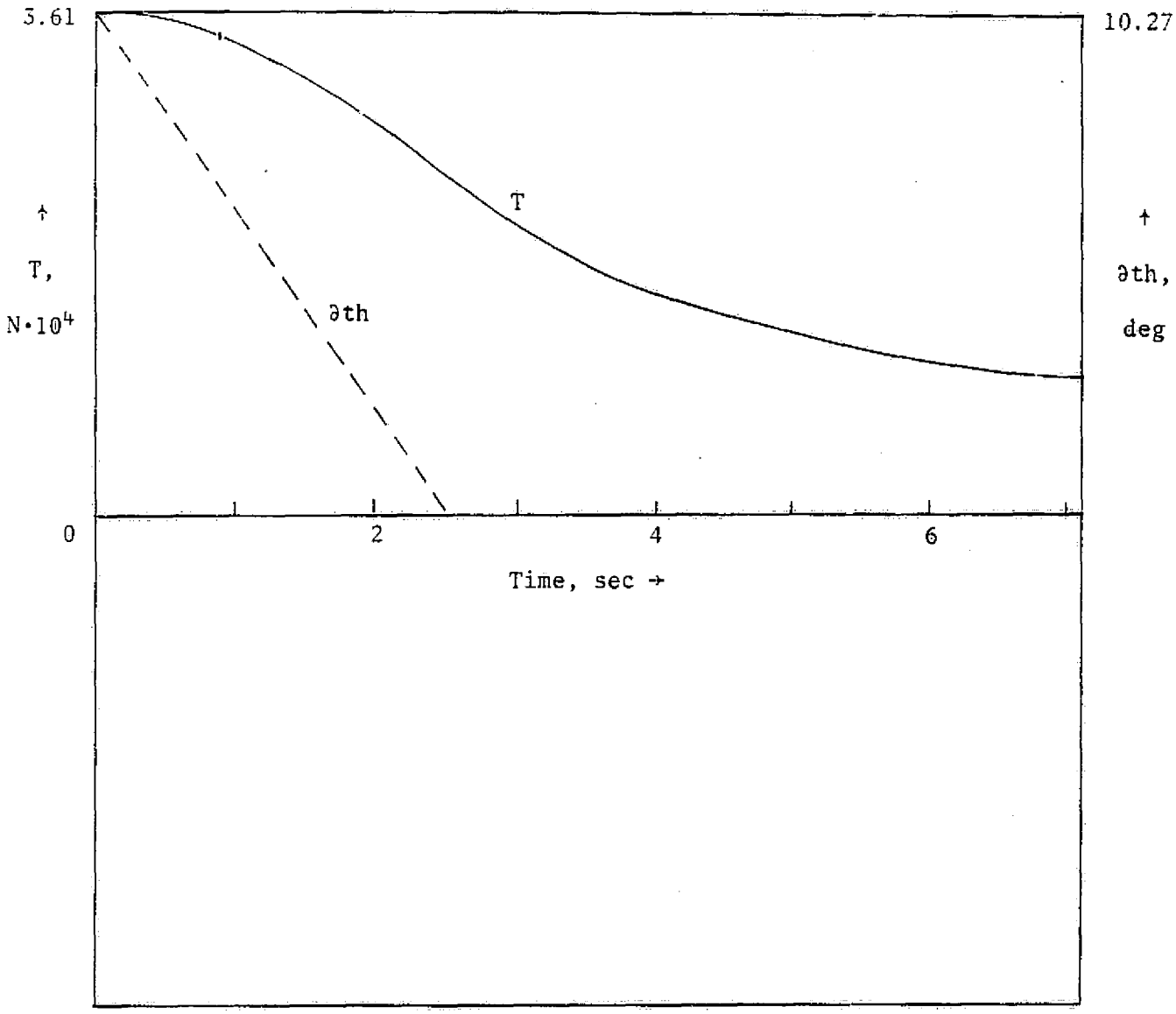

Figure 10(c). Flare response, -3° glide slope: thrust and throttle; no wind gust, controller 3.

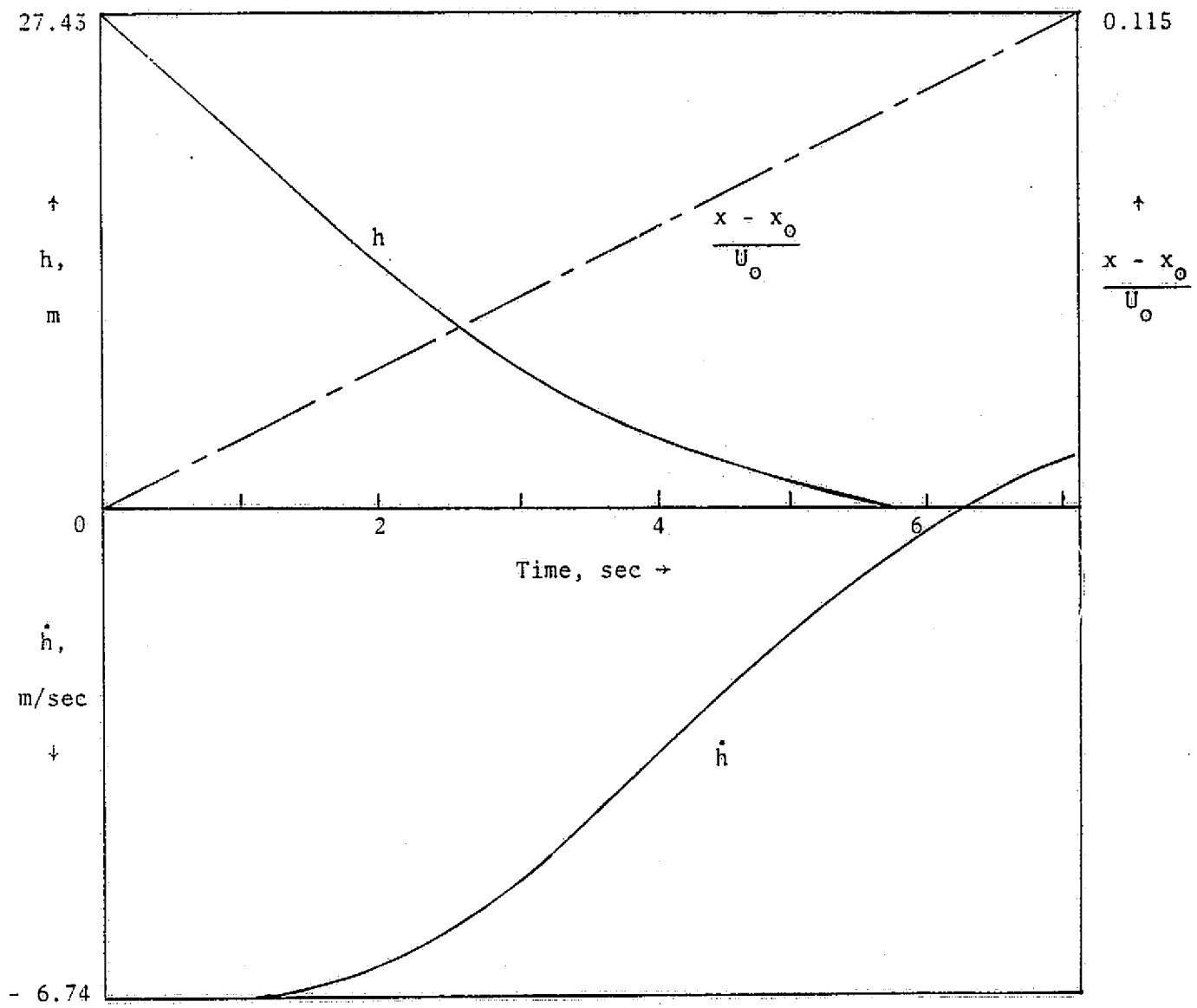

Figure 11(a). Flare response, -6° glide slope: altitude, sink rate, and horizontal dispersion; no wind case, controller 3.

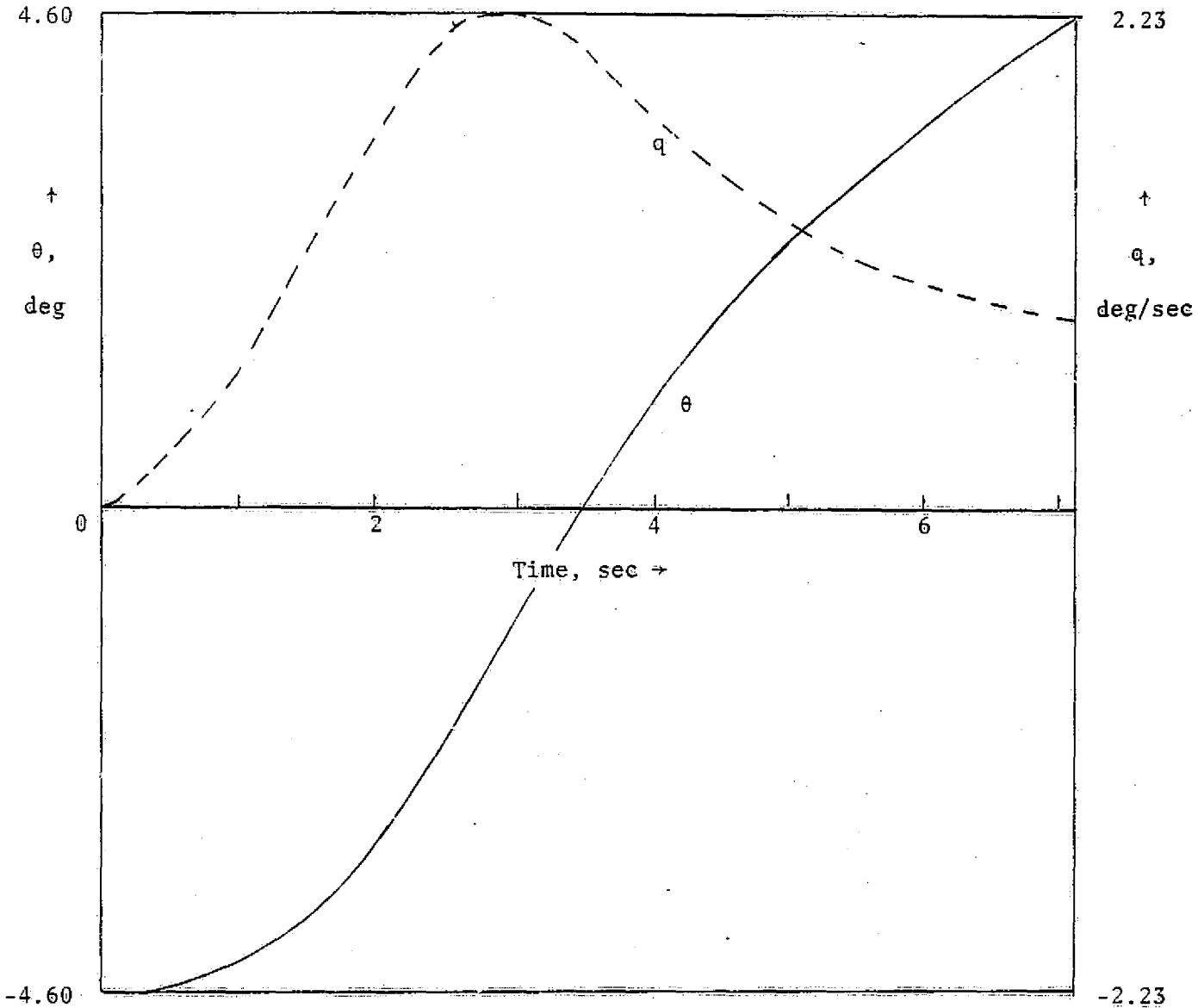

Figure 11(b). Flare response, -6° glide slope: pitch and pitch rate; no wind case, controller 3.

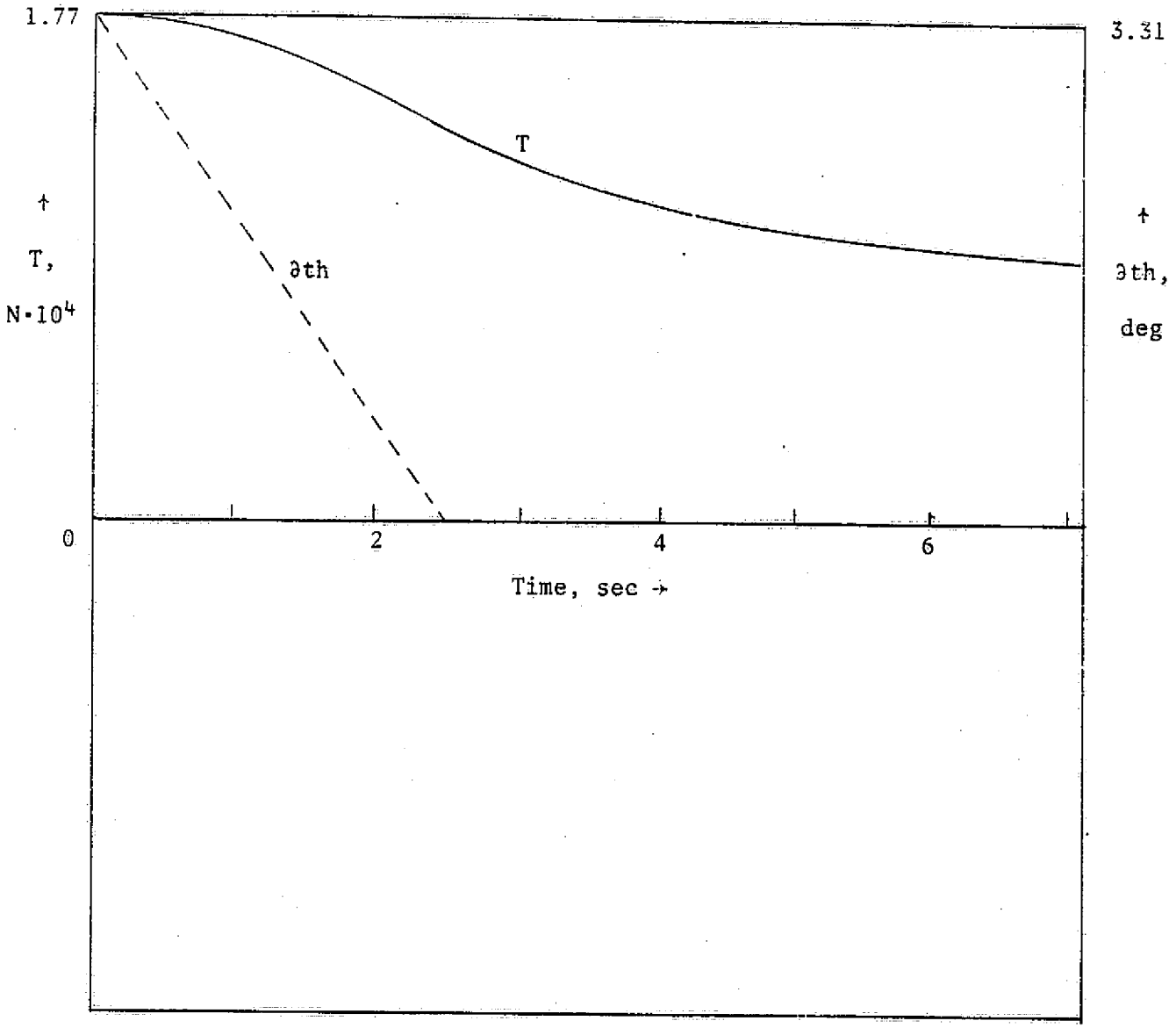

Figure 11(c). Flare response, -6° glide slope: thrust and throttle; no wind case, controller 3.